Design, Synthesis, and DNA Binding Properties of Photoisomerizable Azobenzene−Distamycin Conjugates: An Experimental and Computational Study

ARTICLE *in* BIOCONJUGATE CHEMISTRY · DECEMBER 2008

Impact Factor: 4.51 · DOI: 10.1021/bc800130u · Source: PubMed

6 AUTHORS, INCLUDING:

Usharani Dandamudi
Central Food Technological Research Instit…
27 PUBLICATIONS **314** CITATIONS
SEE PROFILE

Ananya Paul
Georgia State University
14 PUBLICATIONS **188** CITATIONS
SEE PROFILE

Susmita De
National Institute of Technology Calicut
25 PUBLICATIONS **177** CITATIONS
SEE PROFILE

Santanu Bhattacharya
Indian Institute of Science
238 PUBLICATIONS **6,647** CITATIONS
SEE PROFILE

Design, Synthesis, and DNA Binding Properties of Photoisomerizable Azobenzene−Distamycin Conjugates: An Experimental and Computational Study

Sumana Ghosh,[‡] Dandamudi Usharani,[§] Ananya Paul,[‡] Susmita De,[§] Eluvathingal D. Jemmis,[†,§] and Santanu Bhattacharya*[,‡,||]

Department of Organic Chemistry and Department of Inorganic and Physical Chemistry, Indian Institute of Science, and Chemical Biology Unit, Jawaharlal Nehru Centre of Advanced Scientific Research, Bangalore 560 012, India. Received March 30, 2008; Revised Manuscript Received August 26, 2008

Here, we present the synthesis, photochemical, and DNA binding properties of three photoisomerizable azobenzene−distamycin conjugates in which two distamycin units were linked via electron-rich alkoxy or electron-withdrawing carboxamido moieties with the azobenzene core. Like parent distamycin A, these molecules also demonstrated AT-specific DNA binding. Duplex DNA binding abilities of these conjugates were found to depend upon the nature and length of the spacer, the location of protonatable residues, and the isomeric state of the conjugate. The changes in the duplex DNA binding efficiency of the individual conjugates in the dark and with their respective photoirradiated forms were examined by circular dichroism, thermal denaturation of DNA, and Hoechst displacement assay with poly[d(A-T).d(T-A)] DNA in 150 mM NaCl buffer. Computational structural analyses of the uncomplexed ligands using ab initio HF and MP2 theory and molecular docking studies involving the conjugates with duplex d[(GC(AT)$_{10}$CG)]$_2$ DNA were performed to rationalize the nature of binding of these conjugates.

INTRODUCTION

The distamycin and netropsin are well-known naturally occurring DNA minor groove binders (*1, 2*). These are known to selectively recognize A/T-rich base pairs via hydrogen bonding with base pairs together with van der Waals and electrostatic interactions with DNA (*3, 4*). Consequently, there is a continuing effort to modify natural distamycin A to enhance its sequence recognition and binding affinity with double-stranded (ds) DNA. In the past few years, various synthetic strategies have been developed to modify the distamycin scaffold to enhance the recognition efficiency together with mixed base-pair reading capacity. Thus, various new types of DNA binding molecules were designed to enhance and alter sequence specificity of distamycin to any desired target stretch of ds-DNA (*5, 6*). Another strategy to achieve improved DNA binding involved dimerization of DNA minor groove binders (MGB) (*7*−*9*). Although the gain in binding constant is often not as much as expected from dimerization, these modified ligands were found to recognize an extended stretch of 15−16 consecutive AT/GC base pairs with higher binding constant values (*10*−*12*).

We have been working on different DNA binding/cleaving molecules (*13*−*18*) and, in particular, with the distamycin analogues including its tail-to-tail dimers for improving their DNA recognition properties (*19*−*21*). We also reported the thermal stabilization of DNA upon conjugation of distamycin with oligodeoxynucleotides (*22*). In another effort, we have described the differences in their photochemical and DNA binding abilities of distamycin dimers connected through isomeric 2,2' and 4,4'-dialkoxyazobenzene units (*23*). Herein we introduce the conjugates possessing an azobenzene moiety to which two distamycin arms has been connected via different types of linkages. The reason for choosing the azobenzene is due to its nearly reversible photoisomerization property (*24*). The light-induced isomerization of azobenzene is accompanied by significant changes in geometry and polarity of the chromophore (*25*). This unique property has already been widely exploited in various side chains and backbones of peptides, oligonucleotides, sugar scaffolds, and phospholipids to modify and regulate various biological processes (*26*−*30*). Indeed, an azobenzene group was also tethered into many transcription factors and at various positions of the T7-promoter site to modulate the transcription machinery in the presence of light (*31, 32*).

Here, we present the syntheses of three distamycin−azobenzene conjugates that vary in terms of the electronic nature of the linkage and in the length and the type of the spacer that connects them. The dimeric distamycin−azobenzene conjugates, **1**, **2**, and **3**, were synthesized using two different distamycin analogues, **Dist-1** and **Dist-2**. These distamycin analogues have an identical number of amide bonds for interaction with DNA bases, but they differ in terms of the number of N-methyl pyrrole rings and with respect to the position of partial charge developed along the distamycin backbone at physiological pH. So in the case of **1a**, **Dist-1** analogue is covalently connected to the 4,4′ (para) position of the electron-donating alkoxy substituted azobenzene moiety. On the other hand for ligands **2a** and **3a**, **Dist-1** and **Dist-2** units are covalently conjugated to the 4,4- position of the azobenzene core with *electron-withdrawing* carboxamido substituents, respectively, to furnish azobenzene−distamycin conjugates with a long or short spacer (Figure 1). We have examined the influence of the azobenzene moiety on the

* For correspondence. E-mail: sb@orgchem.iisc.ernet.in, Phone: +(91)-80-2293-2664, Fax: +(91)-80-2360-0529.

[‡] Department of Organic Chemistry, Indian Institute of Science.

[§] Department of Inorganic and Physical Chemistry, Indian Institute of Science.

[†] Present address: Indian Institute of Science Education and Research, Thiruvananthapuram, CET Campus, TVM 695016, Kerala, India.

[||] Jawaharlal Nehru Centre of Advanced Scientific Research.

10.1021/bc800130u CCC: $40.75
Published on Web 11/08/2008

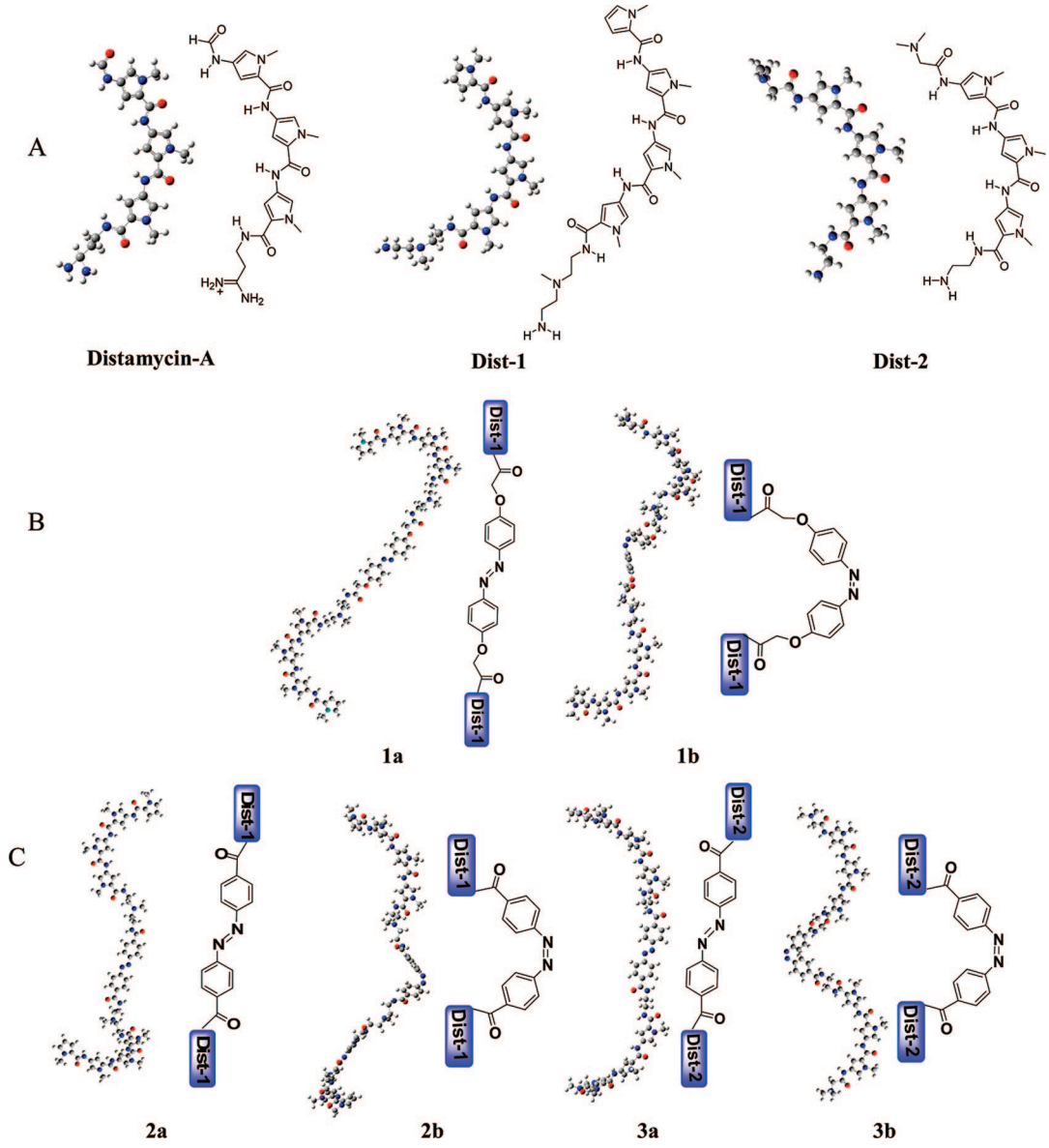

Figure 1. Chemical and optimized structures at the HF/3−21G level of theory of natural distamycin A, distamycin analogues, **Dist-1** and **Dist-2** (A), 4,4′-bis-alkoxyazobenzene containing **Dist-1** in **1a** (trans) and **1b** (cis) (B), 4,4′-bis-carboxamidoazobenzene containing **Dist-1** in **2a** (trans) and **2b** (cis); and (C) **Dist-2** in **3a** (trans) and **3b** (cis) linked via short spacer.

distamycin binding of the DNA minor groove and the changes in ds-DNA binding upon photoisomerization of the conjugate.

By examining the binding properties of these azobenzene−distamycin compounds (**1**, **2**, and **3**) with duplex DNA before and after photoillumination, we sought to address the following questions. Does the incorporation of azobenzene moiety in conjugates **1**, **2**, and **3** interfere with distamycin binding on DNA minor grooves in the ground state? How do the binding of distamycin arms vary upon changing the electronic nature of substituent (alkoxy vs carboxamido) on the azobenzene, e.g., between ligands **1** and **2**? How do ds-DNA binding characteristics vary with linker lengths between the long spacer based **2** and the short spacer based **3** for carboxamido-substituted azobenzene−distamycin conjugates? Finally, how much influence does the photoisomerization impart on the DNA binding properties of such azobenzene−distamycin conjugates?

We first illuminated ligand **1** at ∼360 nm and ligands **2** and **3** at ∼330 nm in solution to produce the corresponding photoisomeric forms. DNA binding properties and the changes in DNA binding efficiencies of individual conjugates in both their ground and photoisomerized states were studied by circular dichroism spectroscopy, thermal denaturation studies, and Hoechst displacement assay. We have also compared with **Dist-1** the DNA binding affinity of different photoirradiated forms of **1**, **2**, and **3** (in their photostationary state) designated as **1***, **2***, and **3***, respectively, to evaluate the effect of incorporation of azobenzene on DNA binding. The experimental results were then analyzed by ligand docking studies using duplex $d[(GC(AT)_{10}CG)]_2$ DNA scaffold. Both experimental and theoretical studies indicate that the duplex DNA binding is highly dependent on the linker length between the azobenzene and the distamycin. The linker length also influences the hydrogen bonding contacts between the pyrrole amide with DNA bases and helps to achieve proper shape complimentarity with the double helical DNA axis.

EXPERIMENTAL PROCEDURES

Synthesis. All reagents used in this study were of the highest purity available and were used without purification. Distamycin analogue, **Dist-1**, is a tetra *N*-methylpyrrole based oligopeptide, which has been synthesized and shown to interact with ds-DNA

along the minor groove surface as reported earlier (*33*). Compounds **4**, **8**, and **10** were prepared as described earlier (*33*−*36*).

4,4′-Dihydroxyazobenzene (*4*). A mixture of KOH (50 g, 760 mmol), *p*-nitrophenol (10 g, 72 mmol), and water (10 mL) was first heated to 120 °C and left to stand in a heating bath for 1 h. When the temperature slowly rose to 195−200 °C, the reaction vigorously started with the formation of large number of bubbles to give a brown viscous liquid. After the reaction was completed, the mixture was cooled and the products were dissolved in water. This afforded a dark red solution, which was acidified to pH 3 with concentrated HCl and extracted with ethyl acetate. Combined ethyl acetate extracts were dried over anhydrous Na_2SO_4 and removed to dryness under reduced pressure. Residue was recrystallized several times with distilled ethanol to give yellow crystals of **4** (*35*). The isolated yield was 4.0 g (43%). IR (cm^{-1}): 1600. ^1H NMR (300 MHz, DMSO-d_6) δ (ppm): 6.9 (d, $J = 9$ Hz, 4H), 8.2 (d, $J = 9$ Hz, 4H). ESI MS (positive ions): *m*/*z* calcd. 215.2 $[M + H]^+$, found 215.2 $[M + H]^+$.

4,4′-Bis(1-(carbomethoxy)methoxy)azobenzene (*5*). Methyl bromoacetate (1.2 mL, 13.0 mmol) was added to a mixture of 4,4′-dihydroxyazobenzene (0.8 g, 3.8 mmol), K_2CO_3 (5.4 g, 26.0 mmol), and 18-crown-6 (0.12 g, 0.46 mmol) in dry acetone (20 mL), and the mixture was refluxed for 15 h. The reaction mixture was then cooled to room temperature, filtered, and evaporated. The residue was dissolved in ethyl acetate, washed with water, and dried over anhydrous $MgSO_4$. The solvent was removed to dryness, and the crude product was purified by column chromatography over silica gel using EtOAc/hexane eluent (20:80) followed by EtOAc/hexane (30:70). This furnished 1.0 g of **5** as a yellow-colored solid (75%). IR (cm^{-1}): 1756.8, 1598.7. ^1H NMR (300 MHz, $CDCl_3$) δ (ppm): 3.83 (s, 6H), 4.7 (s, 4H), 7.01 (d, $J = 8.7$ Hz, 4H), 7.88 (d, $J = 9.0$ Hz, 4H). ESI MS (positive ions): *m*/*z* calcd. 359.4 $[M + H]^+$, found 359.4 $[M + H]^+$.

4,4′-Bis(1-(carboxylic acid)methoxy)azobenzene (*6*). Compound **5** (1.0 g, 2.8 mmol) was dissolved in 20 mL THF. A solution of 2.2 g (56 mmol) of NaOH in 50 mL water was added into the above solution and the mixture was heated under reflux for 2 h. Then, THF was removed under reduced pressure, and the remaining solution was cooled and acidified with 0.5 N HCl. The yellow solid that precipitated was filtered and dried over anhydrous P_2O_5. This furnished 0.74 g of acid, **6** (80% yield). IR (cm^{-1}): 3438.5, 1734.6, 1707.6, and 1600.6. ^1H NMR (300 MHz, DMSO-d_6) δ (ppm): 4.8 (s, 4H), 7.08 (d, $J = 9$ Hz, 4H), 7.82 (d, $J = 9.3$ Hz, 4H). ESI MS (positive ions): *m*/*z* calcd. 330.27 $[M]^+$, found 330.2 $[M]^+$.

4,4′-Bis(1-(chlorocarbonyl)methoxy)azobenzene (*7*). Compound **6** (150 mg, 0.5 mmol) was dissolved in 5.0 mL dry THF and into that 15 mL of distilled $SOCl_2$ was added under ice−cold condition. The reaction mixture was refluxed for 3 h. After that, both solvent and $SOCl_2$ were evaporated under vacuum. This resulted in the formation of a gummy acid chloride in ∼70% isolated yield. The acid chloride was directly used in the next step. IR (cm^{-1}): 1758.8, 1599.6.

4,4′-Bis[(1-carboxamide-*N*-2-2-[(2-aminoethyl)(methyl)amino[(1-methyl-4[(1-methyl-4[(1-methyl-4 [(1-methyl-1*H*-pyrrol-2-yl)carbonyl]amino-1*H*-pyrrol-2-yl)carbonyl]amino-1*H*-pyrrol-2-yl)carbon-yl]amino-1*H*-2-pyrrolecarboxamide]methoxy)azobenzene (*1*). The distamycin derivative, **Dist-1**, (0.6 g, 1.1 mmol) was dissolved in 15 mL of dry THF, and into it, 150 μL of *N*,*N*′-diisopropyl-*N*-ethylamine (DIEA) (0.9 mmol) was added. Acid chloride, **7**, (100 mg, 0.3 mmol) was dissolved in dry THF and added slowly into the above solution. The reaction mixture was stirred at room temperature for 4 h. The solvent was evaporated and the reaction mixture was adsorbed in neutral Al_2O_3 and eluted with $CHCl_3$ followed by MeOH/$CHCl_3$ (2:98) mixture. This furnished **1** as a yellow solid (0.2 g) in 53% isolated yield. ^1H NMR (300 MHz, DMSO-d_6) δ (ppm): 2.23 (s, 6H), 2.49 (s, 8H), 3.78, 3.83, 3.84, 3.87 (s, 12H), 4.56 (s, 4H), 6.04 (dd, $J_1 = 2.4$ Hz, $J_2 = 4.0$ Hz, 1H), 6.86 (m, 1H), 6.9−6.94 (m, 2H), 7.03 (bs, 2H), 7.07−7.1 (dd, 4H, $J_1 = 8.7$ Hz), 7.163 (bs, 1H), 7.22 (bs, 2H), 7.77−7.8 (dd, 4H, $J_1 = 8.7$ Hz), 9.8, 9.86, 9.9 (bs, 8H). ^{13}C NMR (125 MHz, DMSO-d_6) δ (ppm): 36.1, 42.0, 55.96, 72.52, 104.2, 104.73, 106.68, 108.16, 112.66, 115.3, 117.9, 118.45, 121.25, 122.2, 122.8, 124.1, 125.45, 126.32, 128.16, 145.56, 161.3, 163.2, 164.6, 167.22, 168.7, 169.88; ESI MS (positive ions): *m*/*z* calcd. 1475.58 $[M]^+$, 738.3 $[(M + H)/2]^+$, found 1475.6 $[M]^+$ (20%), 738.6 $[(M + H)/2]^+$, (100%). Anal. Calcd. for $C_{74}H_{86}N_{22}O_{12}.H_2O$: C, 59.5; H, 5.94; N, 20.63. Found: C, 59.1; H, 6.3; N, 20.3.

Azobenzene 4,4′-Dicarboxylic Acid (*8*). *p*-Nitrobenzoic acid (15 g, 67.5 mmol) and NaOH (50 g, 1.25 mmol) were mixed in water (225 mL), and the solution was heated on a water bath until the solid dissolved; hot aqueous glucose (100 g in 150 mL of water) was then added slowly into the above mixture at 50 °C whereupon a yellow precipitate was obtained, which immediately changed to a brown solution upon further addition of glucose. This reaction was highly exothermic. Then, a stream of air was passed into the mixture for 3 h and a light brown precipitate was obtained. This was filtered, dissolved in water, and acidified with acetic acid (25 mL) whereupon a light pink precipitate was obtained. This was filtered, washed with plenty of water (300 mL), and dried in a desiccator to obtain **8** (yield 9 g, 80%) as a brownish orange powder (*36*). ^1H NMR (300 MHz, DMSO-d_6) δ (ppm): 8.15 (d, 4H, $J = 8.7$ Hz), 7.99 (d, 4H, $J = 8.7$ Hz).

Azobenzene 4,4′-Dicarbonyl Chloride (*9*). To a suspension of **8** (1 g, 3.7 mmol) in 20 mL of 1,2-dichloromethane was added 2.0 g PCl_5 at 0 °C and then refluxed for 2 h. This afforded bright red crystals, which were filtered and recrystallized repeatedly from toluene to afford **9** (*36*) (0.84 g, 75%). IR (ν, cm^{-1}): 1776.12 (CO) and 1600 (N═N); ^1H NMR (300 MHz, $CDCl_3$) δ (ppm): 8.1 (d, $J = 8.7$ Hz, 4H), 8.32 (d, $J = 8.4$ Hz, 4H).

***N*-Methyldiethylenetriamine-Based Bis-Carboxamido Azobenzene−Distamycin Conjugate (*2*). Dist-1** (0.14 g, 0.30 mmol) was dissolved in 3.0 mL dry THF and into it DIEA (54 μL, 0.18 mmol) was added. Acid chloride, **9**, (18 mg, 0.06 mmol) dissolved in 4 mL dry THF was added slowly into the above solution. The reaction mixture was then stirred at room temperature for 12 h. The solvent was evaporated, and the reaction mixture was adsorbed in neutral alumina and first eluted with $CHCl_3$ followed by a mixture of MeOH/$CHCl_3$ (2:98) mixture. This furnished 0.04 g of **2** as an orange solid in overall 50% yield. ^1H NMR (300 MHz, $CDCl_3$) δ (ppm): 2.4 (bs, 6H), 2.7 (bs, 8H), 3.4−3.45, 3.55 (m, 8H), 3.71, 3.73, 3.86, 3.97 (s, 12H), 6.1 (dd, $J_1 = 2.4$ Hz, $J_2 = 3.6$ Hz, 1H), 6.64 (bs, 2H), 6.71, (bs, 1H), 6.76 (bs, 1H), 6.92 (bs, 2H), 7.1 (bs, 1H), 7.26 (bs, 1H), 7.58 (d, $J = 7.8$ Hz, 4H), 7.7 (d, $J = 8.4$ Hz, 4H). ^{13}C NMR (125 MHz, DMSO-d_6) δ (ppm): 36.5, 56.7, 105.2, 113.1, 118.3, 118.9, 122.6, 123.0, 123.3, 125.9, 126.8, 128.6, 128.9, 152.0, 153.5, 159.2, 162.0, 166.0, 167.22, 168.7, 169.88. ESI MS (positive ions): *m*/*z* calcd. 1415.53 $[M]^+$, found 1415.8 $[M]^+$. Anal. Calcd. for $C_{72}H_{82}N_{22}O_{10}.H_2O$: C, 60.32; H, 5.91; N, 21.49. Found: C, 59.9; H, 6.27; N, 21.1.

Azasuccinimidyl-1-methyl-4-[(1-methyl-4-nitro-1*H*-2-pyrrolyl)carbonyl]amino-1*H*-2-pyrrolecarboxylate (*11*). 1-Methyl-4-[(1-methyl-4-nitro-1*H*-2-pyrrolyl)carbonyl]amino-1*H*-2-pyrrole carboxylic acid **10** (0.15 g, 0.36 mmol) was dissolved in DMF (1 mL) and cooled in an ice bath. *N*-Hydroxysuccinimide (54 mg, 0.47 mmol) was added into the solution followed by dicyclohexyl carbodiimide (100 mg, 0.47 mmol). The

resulting solution was stirred for 1 h, first at 0 °C and then at room temperature for another 6 h. The precipitated dicyclohexyl urea was filtered off, and the filtrate was diluted with EtOAc. The EtOAc and DMF were evaporated under vacuum to obtain the succinimide ester of pyrrole carboxylic acid derivative **11** as a pure solid. The isolated yield was 0.15 g (80%). However, the product was found to be hydrolytically very unstable, and due to this, the product **11** was directly used for the next step without further purification.

2-*tert*-Butoxycarbonylamino-1-aminoethane (*12*). Ethylene diamine (3.35 mL, 50 mmol) was dissolved in dry THF and cooled in an ice bath. Triethyl amine (1.74 mL, 12.5 mmol) was added into it followed by dropwise addition of di *t*-butyl dicarbonate (2.7 g, 12.5 mmol). The reaction mixture was stirred for 12 h at room temperature. After that, the solvent was removed by rotary evaporation and the resultant mass was dissolved in ethyl acetate. The EtOAc layer was washed successively with 5 mL water and 5 mL brine and dried over anhydrous Na_2SO_4. The resultant solution was evaporated and adsorbed in neutral alumina column. It was first eluted with $CHCl_3$, followed by (1:99) MeOH/$CHCl_3$ mixture to obtain **12** as a pure solid. The isolated yield was 1.5 g (75%). ^{1}H NMR (300 MHz, $CDCl_3$) δ (ppm): 1.45 (s, 9H), 1.98 (bs, 2H), 3.16−3.21 (q, $J_1 = 5.4$ Hz, $J_2 = 5.1$ Hz, 2H), 5.03 (bs, 2H).

***N*-2[*tert*-Butoxycarbonylamino-1-aminoethane[1-methyl-4-[(1-methyl-4-nitro-1*H*-pyrrol-2-yl) carbonyl]amino-1*H*-2-pyrrole carboxamide (*13*).** A solution of **11** (0.2 g, 0.4 mmol) in dry THF was added dropwise into a solution of 12 (0.072 g, 0.45 mmol) in THF at room temperature. A catalytic amount of triethylamine was added and the resulting mixture was stirred at room temperature for 4 h. At the end of 4 h, the solvent was evaporated and directly adsorbed on silica. The resulting mixture was purified by eluting column with $CHCl_3$ followed by MeOH/$CHCl_3$ (3:97) mixture. This yielded 0.13 g of **13** (60%). ^{1}H NMR (300 MHz, $CDCl_3$) δ (ppm): 1.44 (s, 9H), 3.35−3.5 (m, 4H), 3.71, 3.82, 3.91 (s, 9H), 6.54 (s, 1H), 6.7 (s, 1H), 7.22 (bs, 2H), 7.6 (s, 2H), 7.74, 7.77, 8.12, 8.2 (bs, 4H). ESI MS (positive ions): *m*/*z* calcd. 556.7 $[M]^+$, found 557 $[M]^+$.

***N*-2[*tert*-Butoxycarbonylamino-1-aminoethane[1-methyl-4-[(1-methyl-4-[bromoethanamido]-1*H*-pyrrol-2-yl)carbonyl]amino-1*H*-2-pyrrolecaroboxamide (*14*).** 200 mg (0.36 mmol) of **13** was dissolved in 1.5 mL of dry DMF and hydrogenated over 90 mg of Pd/C (5%) for 20 h at room temperature. The catalyst, Pd/C, was filtered off and the residue was washed twice with 1 mL each of dry DMF. The combined filtrate and washings were collected together and mixed with 0.3 mL (1.7 mmol) of DIEA and was cooled to 0 °C. To this solution, 0.1 mL (1.0 mmol) of bromoacetyl bromide was added, and the resultant solution was stirred for 2 h at 0 °C and then at room temperature for 8 h. At the end of this period, the reaction mixture was washed with water and extracted with ethyl acetate. The crude reaction mixture obtained upon evaporation of ethyl acetate was adsorbed on silica gel and purified by column chromatography upon elution with $CHCl_3$ followed by MeOH/$CHCl_3$ (4:96) mixture. The product was isolated as a yellow solid. The isolated yield was 93 mg (40%). ^{1}H NMR (300 MHz, $CDCl_3$) δ (ppm): 1.4 (s, 9H), 3.3−3.45 (m, 4H), 3.83, 3.85, 3.87 (s, 9H), 3.96 (s, 2H), 6.54 (bs, 2H), 6.7 (s, 1H), 7.1 (s, 1H), 7.21 (bs, 2H), 8.2, 8.5, 8.63 (bs, 4H). ESI MS (positive ions): *m*/*z* calcd. 669.0 $[M + Na]^+$, 671.0 $[M + Na]^+$; found 669.2 $[M + Na]^+$, 671.2 $[M + Na]^+$.

***N*-2[*tert*-Butoxycarbonylamino-1-aminoethane[1-methyl-4-[(1-methyl-4-[dimethylaminoethanamido]-1*H*-2-pyrrolyl) carbonyl]amino-1*H*-2-pyrrolecarboxamide (*15*).** Compound **14** (0.05 g, 0.08 mmol) was dissolved in dry MeOH, the solution was cooled in an ice−water bath, and excess dimethylamine gas was passed into it in a screw-top pressure tube. The resultant mixture was then heated at 70 °C for 12 h. Excess dimethylamine was evaporated, and the residual mass was dissolved in ethyl acetate, washed with saturated $NaHCO_3$ solution, water and brine, and finally dried over anhydrous Na_2SO_4. The gummy mass obtained upon evaporation of solvents was purified by column chromatography on alumina using $CHCl_3$ followed by MeOH/$CHCl_3$ (2:98) mixture as eluent. This afforded **15** as a gum (35 mg, 75%). ^{1}H NMR (300 MHz, $CDCl_3$) δ (ppm): 1.4 (s, 9H), 2.3 (s, 6H), 3.05 (s, 2H), 3.3 (m, 2H), 3.45 (m, 2H), 3.84, 3.87, 3.9 (three s, 9H), 6.56 (s, 1H), 6.6 (s, 1H), 6.9 (s, 1H), 7.0 (s, 1H), 7.16 (s, 1H), 7.22 (s, 1H), 5.3, 6.8, 8.03, 8.16, 8.94 (bs, 5H). ESI MS (positive ions): *m*/*z* calcd. 611.8 $[M]^+$, found 612 $[M]^+$.

***N*-2[Diaminoethane[1-methyl-4-[(1-methyl-4-[bromoethanamido]-1*H*-2-pyrrol-yl)carbonyl]amino-1*H*-2-pyrrolecarboxamide (*16*).** To a solution of **15** (60 mg, 0.1 mmol) in dichloromethane (2 mL), an equal volume of trifluoroacetic acid (TFA) (2 mL, 26 mmol) was added into it under cold condition (0−5 °C), and the reaction was continued for 2 h at room temperature. After completion of the reaction, the excess TFA and solvent were removed by rotary evaporation. The residue was washed twice with $CHCl_3$ and finally dried to obtain **16** (40 mg, 80%). It was directly used without further purification due to its instability and high reactivity.

Ethylenediamine-Based Bis-Carboxamido Substituted Azobenzene Distamycin Conjugate (*3*). Compound **16** (0.2 g, 0.4 mmol) was dissolved in dry THF and into it 175 μL (1 mmol) diisopropyl ethylamine (DIEA) was added. The resultant mixture was stirred for 15 min at room temperature. Then, again 1.0 mmol of approximately 200 μL DIEA was added. A solution of 4,4′-bis(chlrocarbonyl) azobenzene, **9**, (6 mg, 0.02 mmol) was added dropwise, and the reaction mixture was allowed to stir at room temperature for 12 h. The solvent was evaporated, and the residue was purified by column chromatography on alumina eluted first with $CHCl_3$ followed by MeOH/$CHCl_3$ mixtures (2:98) and (4:96) as eluent. The product was obtained as an orange solid (40 mg, 40%). ^{1}H NMR (300 MHz, $CDCl_3$) δ (ppm): 2.35 (s, 6H), 3.06 (s, 2H), 3.6 (m, 4H), 3.84, 3.87, 3.9 (s, 9 H), 6.88 (s, 1H), 6.93 (s, 1H), 6.98 (s, 1H), 7.14 (s, 1H), 7.23 (s, 2H), 7.96 (d, $J = 8.1$ Hz, 4H), 8.1 (d, $J = 8.4$ Hz, 4H), 8.4, 9.03, 9.26 (bs, 4H). ^{13}C NMR (125 MHz, DMSO-d_6) δ (ppm): 36.5, 56.7, 105.2, 113.1, 118.3, 118.9, 122.6, 122.8, 124.1, 123.0, 123.3, 125.9, 126.8, 128.6, 128.9, 152.0, 153.5, 159.2, 162.0, 166.0, 167.22, 168.7, 169.88. ESI MS (positive ions): *m*/*z* calcd. 1257.34 $[M]^+$, 629.2 $[(M + H)/2]^+$, found 1257.7 $[M]^+$, 629.5 $[(M + H)/2]^+$. Anal. Calcd. for $C_{62}H_{72}N_{20}O_{10}\cdot 0.5H_2O$: C, 58.8; H, 5.81; N, 22.12. Found: C, 58.41; H, 6.23; N, 21.9.

Photoisomerization and UV−vis Analysis. Photoillumination of ligand **1** was carried out using a xenon lamp 450 with light intensity of ca. 40 W, which transmitted light around 360 nm. On the other hand for carboxamido substituted ligands **2** and **3**, photoillumination was done using a water-cooled high-pressure 250 W Hg lamp that transmitted light between 320 and 380 nm after passing through a set of bandpass chemical filters (*37*). The rate of isomerization was measured spectrophotometrically for each ligand (**1**, **2**, and **3**) in DMSO at a given concentration on a UV−vis spectrophotometer at 25 °C. Such spectral analysis as a function of time gave the approximate time required for reaching the photostationary state from each of the azobenzene−distamycin conjugates.

^{1}H NMR Spectroscopy. ^{1}H NMR experiments with each ligand for configurational analysis were carried out at 25 °C using a 300 MHz spectrometer. Individual samples of around 1 mM concentration were taken in d_6-DMSO, and the corresponding changes in the molecular configuration after photoillumination were determined by recording ^{1}H NMR spectros-

Scheme 1[a]

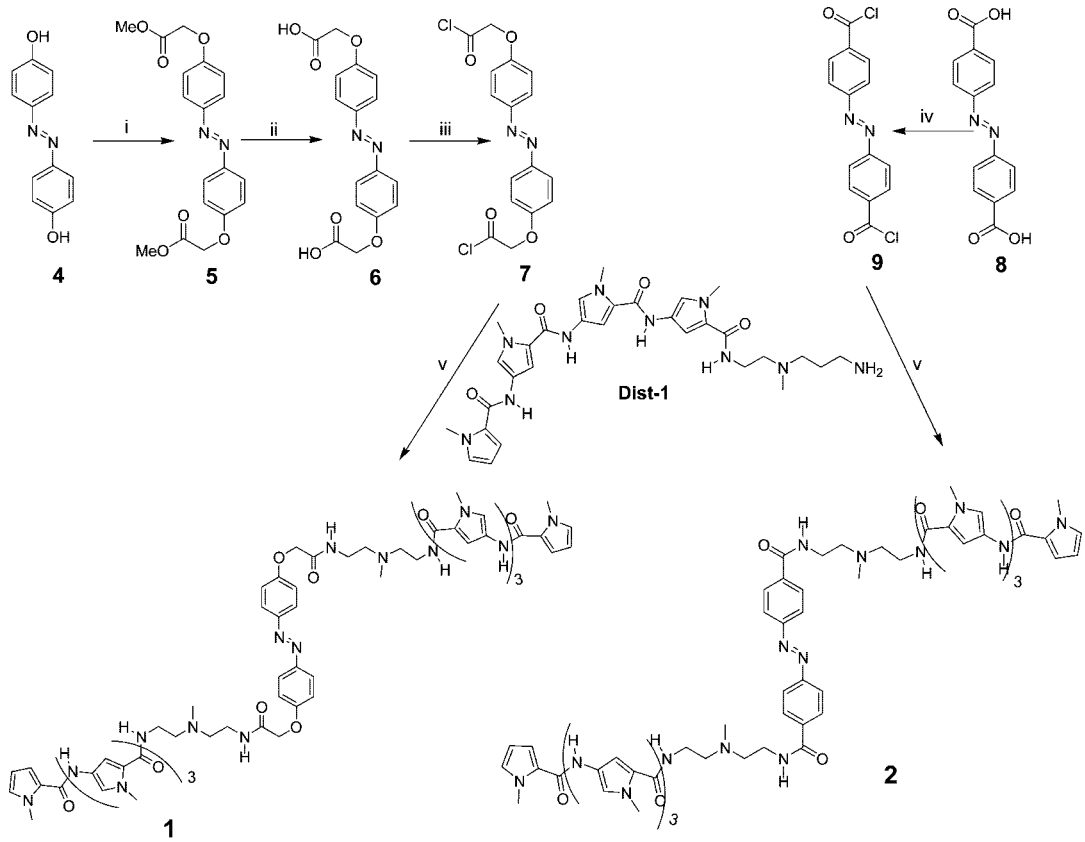

[a] Reagents, conditions, and yields. (i) Methyl bromoacetate, K_2CO_3, 18-crown-6, acetone, reflux, 14 h, 75%; (ii) 0.5 N NaOH, THF, reflux, 2 h, followed by acidification with 0.5 N HCl, 90%; (iii) $SOCl_2$, THF, reflux, 3 h, 90%; (iv) PCl_5, $ClCH_2CH_2Cl$, reflux 2 h, 75%; (v) DIEA, THF, RT, 4 h, 50%.

copy. Integration of the respective azobenzene protons allowed quantitative determination of the percentage of trans and cis forms of each sample in their photostationary states.

Circular Dichroism Spectroscopy. CD spectra were recorded on a spectropolarimeter equipped with a temperature controller. The experiments were performed in NaCl buffer (150 mM NaCl, 0.01 M Tris-HCl, 0.1 mM EDTA buffer at pH 7.4) using 20 μM duplex poly[d(A-T).d(T-A)] with or without the azobenzene−distamycin conjugates at 25 °C. All CD titrations were averaged over two acquisitions and the scan rate was maintained at 50 nm/min with optical cells of path length of 1 cm. Titration was performed under dark and utmost care was taken to minimize the isomerization of azobenzene−distamycin hybrids. The CD values were expressed in millidegree. The changes in ICD intensity at 336 nm were plotted against [ligand]/[DNA] ratio to obtain the concentration of conjugate required to saturate the ds-DNA binding.

Melting Temperature Measurements. The thermal stability of each ligand/ds-DNA complex was assessed from thermal denaturation studies. Using a UV−vis spectrophotometer equipped with a temperature-programmable cell block, the changes in absorbance at 260 nm were followed as a function of temperature. The samples were heated at 0.5 °C/min, and the absorbance values were recorded for every 0.5 °C rise in temperature. All T_m experiments were carried out in NaCl buffer at saturated [ligand]/[DNA] ratios.

Minor Groove-Bound Hoechst Displacement Assay. First, 0.25 μM Hoechst was taken in NaCl buffer and various aliquots of concentrated poly[d(A-T).d(T-A)] solutions were added progressively to saturate Hoechst binding on duplex DNA surface. The fluorescence intensity of Hoechst 33258 increased on binding with duplex poly[d(A-T).d(T-A)]. Each azobenzene−distamycin conjugate was then added individually into saturated solution of the Hoechst−DNA complex, and the displacement of Hoechst from ds-DNA was measured from a decrease in the fluorescence emission intensity at 464 nm (λ_{ex} = 355 nm) at 25 °C. Titration was performed under dark and care was taken to minimize the isomerization of azobenzene−distamycin conjugates. The apparent binding constant (K_{app}) has been calculated as $K_a = K_{app}[L_{50}]$, where K_a indicates the binding constant of Hoechst, which was found to be 1.5×10^7 M^{-1} by Scatchard analysis (*38*) with poly[d(A-T).d(T-A)] in NaCl buffer, and $[L_{50}]$ is the concentration of individual ligand achieving 50% quenching of DNA-bound Hoechst fluorescence.

Computational Details. All the bis-alkoxy and bis-carboxamido substituted azobenzene−distamycin conjugates (**1**−**3**) and **Dist-1** and **Dist-2** analogues were optimized at the HF/3−21G level of theory using *Gaussian 03* (*39*). Single point energies are obtained for the model azobenzenes **17** and **18** at the MP2/6−31+G* level of theory. The Mülliken atomic charges of the optimized ligands (**1**−**3**) obtained from the calculation at the HF/3−21G level of theory are used for docking studies. A nucleotide sequence of $d[GC(AT)_{10}CG]_2$ was generated from the nucgen program of *AMBER 8* (*40*) instead of poly[d(A-T).d(T-A)] DNA. The B-form of DNA built by this procedure is assigned with AMBERff03 force field (*41*) and minimized for 250 steps by steepest decent algorithm and a further 250 steps by the conjugate gradient method to remove the bad strains in the DNA. The modeled ds-DNA was then docked with the optimized ligand structures using AUTODOCK 3.05 version (*42, 43*). The center of the macromolecule is the grid center with grid size of 80 × 80 × 126 and grid spacing of 0.4186 Å. Docking runs were performed using the Lamarckian genetic algorithm (LGA) with some modifications of the docking

Scheme 2[a]

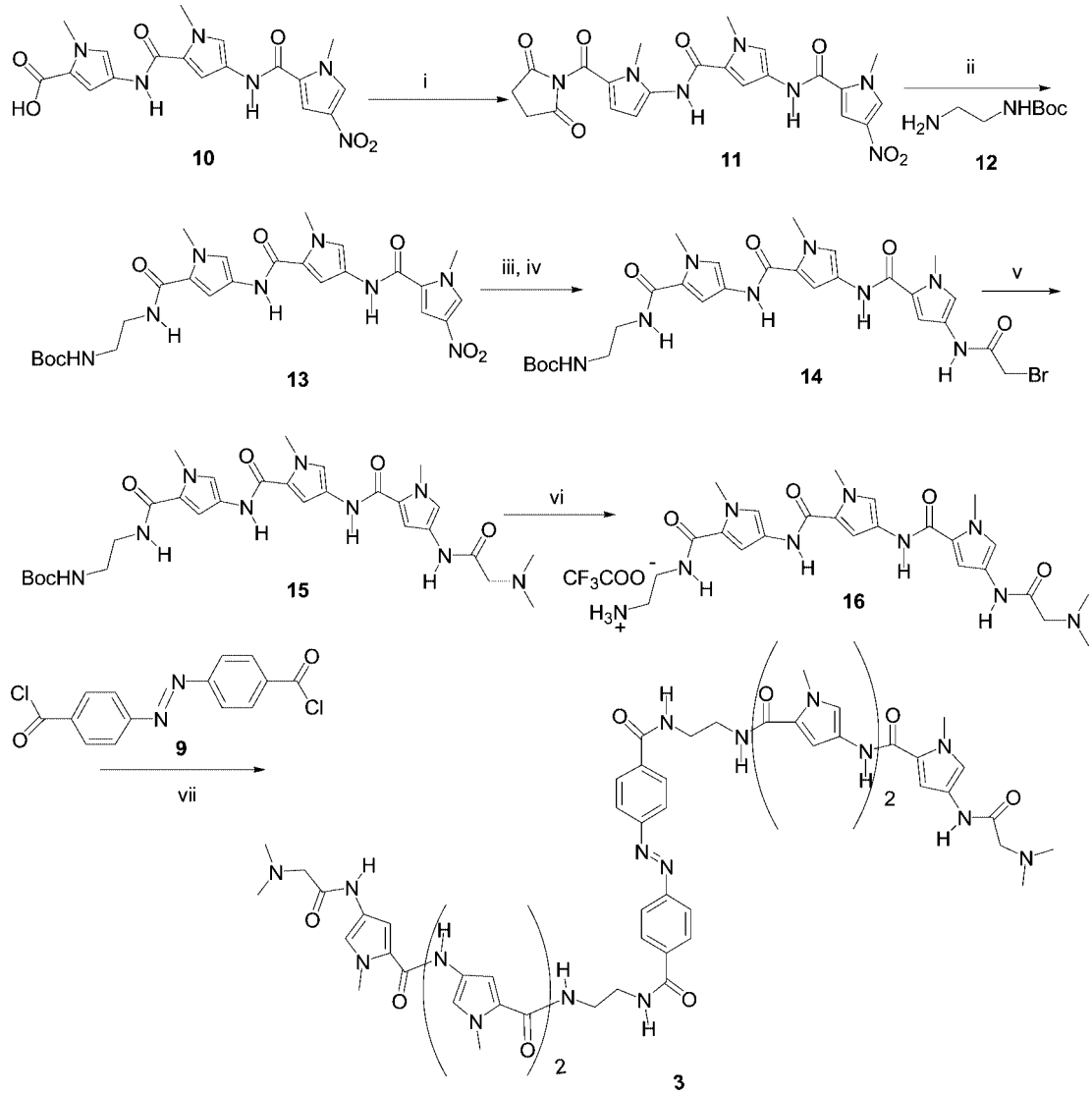

[a] Reagents, conditions, and yields: (i) DCC, NHS, DMF, 0 °C, 1 h, then RT, 6 h, 80%; (ii) THF, RT, 4 h, 60%; (iii) 5% Pd/C, DMF, 20 h, RT; (iv) DIEA, bromoacetyl bromide, 0 °C, 2 h, RT, 40%; (v) $NH(CH_3)_2$, MeOH, 70 °C, 12 h, 75%; (vi) CH_2Cl_2, TFA (1:1), RT, 2 h, 80%; (vii) DIEA, RT, 12 h, 40%.

Table 1. Stabilization Energies (kcal/mol) of Trans Isomers Relative to the Cis Isomers at HF/3–21G Level for Ligands 1−3 and at MP2/6–31+G* Level for the Model Azobenzenes 17 and 18 Using *Gaussian 03*

substitution	*trans*	energy
bis-alkoxide	**1a**	−13.1
	17a	−11.0
bis-carboximido	**2a**	−18.6
	3a	−15.4
	18a	−12.3

Scheme 3. Structures of the Trans and Cis Isomers of Model Azobenzenes 17 (Alkoxy Substituent) and 18 (Carboxamido Substituent)

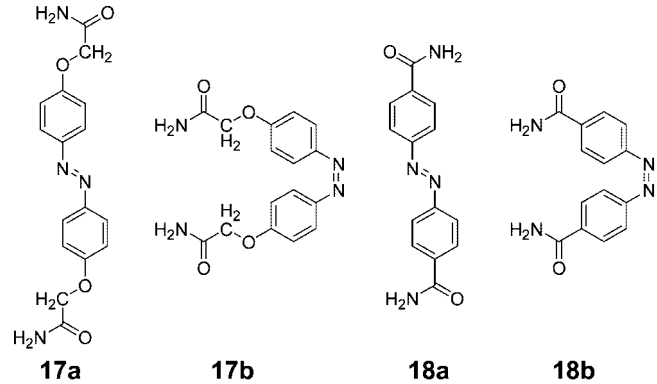

parameters. LGA was used because of the existence of 32−48 rotable bonds in these conjugates and to evaluate the right conjugate−DNA conformation, as it is known to reproduce various experimental ligand−DNA complex structures (*44*−*46*). Docking began with rigid docking of the initial Gaussian optimized structures. Docking of each ligand was derived from 20 different runs that were set to be obtained after a maximum of 500 000 energy evaluations or 25 000 000 generations, to give 20 conformations. The probability that docking solution in the population would undergo a local search was set to 0.06 and the constraint was set to a maximum of 300 iterations per search. The size of local search space (rho) was set to 1.0−0.01. A pseudo-Solis and Wets local search was then used to minimize energy of the population where the population size was set to 50. The elitism number and the rates of gene mutation and gene crossover were 1, 0.02, and 0.08, respectively. The flexible docking procedure was repeated until substantial interactions of the extended binding mode of ligand with DNA were

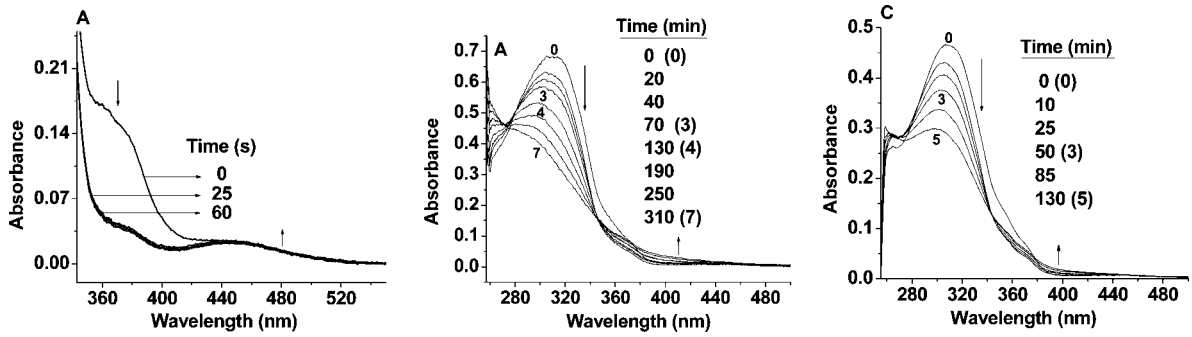

Figure 2. Changes in the absorption spectra of a solution of **1** in DMSO (12 μM, A), **2** (10 μM, B), and **3** (10 μM, C) upon photoillumination at appropriate λ values. Arrows indicate the nature of changes in the observed absorption region of $\pi-\pi^*$ and $n-\pi^*$ transitions of the azobenzene units, respectively.

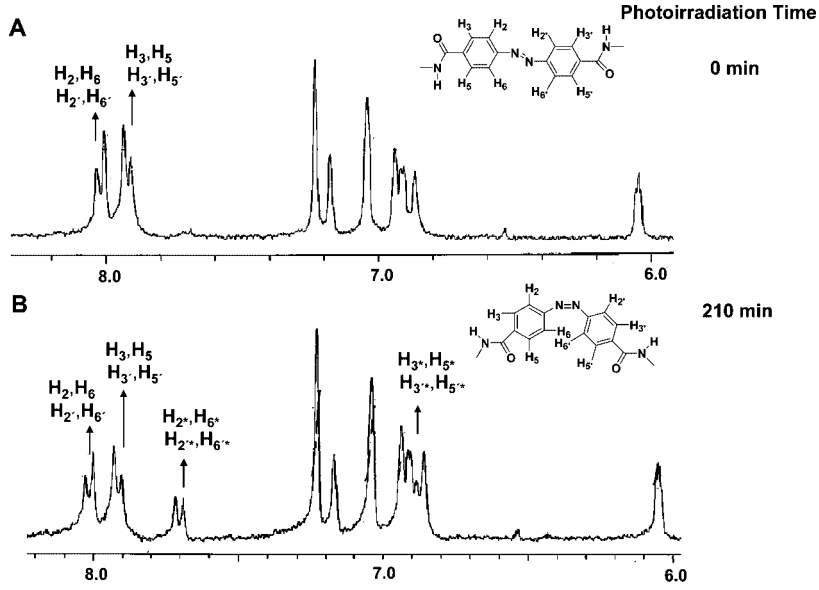

Figure 3. ^{1}H NMR spectra of a d_6-DMSO solution of **2** (1 mM) before (A) and after (B) 210 min of photoillumination at ~330 nm. Chemical shifts of the respective azobenzene protons before and after irradiation are indicated with respect to TMS as standard. The symbol * refers to the sample after irradiation.

obtained. Further, the lowest dock conformation obtained from the flexible docking was again submitted for rigid docking to remove the internal energy of ligand (steric clashes) and retain the hydrogen bonding interaction with ds-DNA bases.

RESULTS AND DISCUSSION

Synthesis. The key starting material **Dist-1** for the synthesis of **1** has been obtained following a procedure described earlier (*19, 33*). The synthesis of **1** began with the alkylation of 4,4′-dihydroxy azobenzene, **4**, with 3.5 equiv of methyl bromoacetate in acetone under reflux conditions as summarized in Scheme 1. The dimethyl ester, **5**, was saponified and then converted to the corresponding acid chloride, **7**. This was then directly used for coupling with 4 equiv of **Dist-1** in dry THF in the presence of Hünig's base at room temperature to furnish **1** as a yellow solid in 50% isolated yield (Scheme 1).

The other starting material azobenzene 4,4′-dicarboxylic acid, **8**, and the corresponding azobenzene 4,4′-dicarbonyl chloride, **9**, were prepared according to the reported procedures (*35*). The synthesis of **2** was accomplished by amide bond formation between the amine tethered distamycin derivative, **Dist-1** (~4 equiv) and **9** in THF at room temperature (Scheme 1). The reaction mixture was chromatographically purified to furnish **2** as an orange solid in 50% isolated yield.

The synthesis of **3** began with tri-*N*-methylpyrrole based nitro acid, **10**, which was synthesized according to a reported procedure (*34*) The acid functionality was activated as NHS ester, **11**, and then directly coupled with **12** in dry THF at room temperature to furnish **13** in ~60% isolated yield. The nitro group present at the N-terminus of the oligopeptide derivative was hydrogenated over Pd/C (5%) in dry DMF followed by capping of the amine functionality by bromoacetyl bromide. The reactive bromide at the N-terminus of the oligopeptide derivative was coupled with dimethyl amine under reflux condition for 12 h to obtain **15**. The *tert*-butoxycarbonyl group present at the C-terminus of oligopeptide was deprotected using TFA to furnish primary amine, **16** (**Dist-2**). Then, ~4 equiv of **16** was directly used for coupling with **9** in dry THF at room temperature to afford **3** in 40% isolated yield (Scheme 2).

Optimized Ligand Structures. The conjugates (*1*−*3*) can give rise to many conformations, which arise due to the change in the dihedral angle around the central C−N═N−C bond of azobenzene. Among various possible conformational isomers, we have calculated the two most significant conformations, cis and trans, at the HF/3−21G level of theory using the *Gaussian 03* program package (*39*). The optimized structures of these ligands are shown in Figure 1. The letters "a" and "b" after structure number indicate trans and cis isomer, respectively. The trans isomers are found to be more stable compared to their respective cis isomers for all the ligands (Table 1). The order of relative stability of the trans isomers with respect to the corresponding cis isomers is **1** (−13.1 kcal/mol) < **3** (−15.4

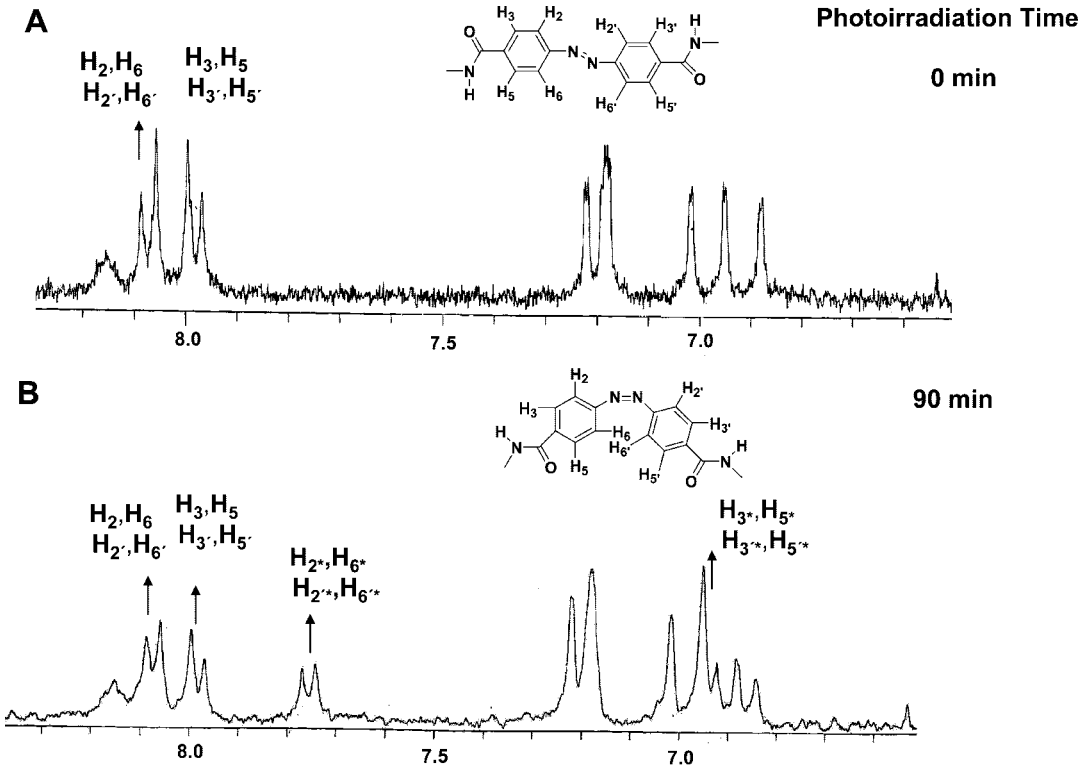

Figure 4. ^{1}H NMR spectra of a d_6-DMSO solution of **3** (1 mM) before (A) and after (B) 90 min of photoillumination at ∼330 nm. Chemical shifts of the respective azobenzene protons before and after irradiation are indicated with respect to TMS as standard. The symbol * refers to the sample after irradiation.

kcal/mol) < **2** (−18.6 kcal/mol). The ligands **1** and **2** feature long linker based **Dist-1**, and ligand **3** has short linker based **Dist-2** (Table 1). It shows that, for a constant linker length, trans isomers are relatively more stable for the electron-withdrawing bis-carboxamido-substituted azobenzenes **2** and **3** as compared to the electron-donating bis-alkoxy-substituted azobenzenes, **1** (Table 1).

In order to understand the electronic effect of the bis-carboxamido versus bis-alkoxy substituents, model azobenzenes **17** and **18** are studied. Structure **17** has OCH_2CONH_2 and structure **18** has $CONH_2$ substituents at the para position to mimic ligands **1** and **2** (or **3**), respectively, (Scheme 3). The trans isomers **17a** and **18a** are more stable in comparison to their respective cis isomers **17b** and **18b** by 11.0 and 12.3 kcal/mol, respectively, at the MP2/6−31+G* level of theory (Table 1). Thus, the trend in the relative energies for ligand **1** is also retained in the model azobenzenes **17** and **18**. This indicates that the bis-carboxamido substituents can stabilize the trans isomer more than the bis-alkoxy substituents.

The azobenzene moiety in the trans isomer is planar, but deviation from planarity is ∼50° in the cis isomer. As a result, the stabilization of the azobenzene π-orbital due to the delocalization in the substituents can only be observed in the trans isomer. The carboxamido group stabilizes the π-molecular orbital of the azobenzene in the trans isomer **18a** by 0.87 eV as compared to the trans isomer **17a** having an alkoxy group. This supports the greater stability of the trans isomers (**2a**, **3a**) of the carboxamido-substituted ligands over the trans isomer (**1a**) of alkoxy-substituted ligands.

Photoisomerization of the Ligands in Solution. As anticipated, the distamycin−azobenzene conjugates photoisomerize upon light illumination. Detailed investigation of the isomerization of azobenzene is important in order to know the composition of the trans and cis isomeric forms at the photostationary state. Accordingly, we followed this for each conjugate by UV−visible and ^{1}H NMR spectroscopy.

UV−vis Analysis. The isomerization process was assessed by irradiation of the distamycin−azobenzene conjugate **1** (12 μM) in DMSO solution at 360 nm (Figure 2A). Upon photoillumination, the absorption band intensity at ∼365 nm due to $\pi-\pi^*$ transition decreased with a considerable blue shift, while the band due to n−π^* transition at ∼450 nm increased. According to previous studies (*35*), the absorption band around 360 nm is due to the trans form of the azobenzene moiety, while that around 450 nm is ascribed to the *c*is form. Therefore, the irradiation indicates transformation of the trans azobenzene to the cis azobenzene moiety. This process continued over a period up to 60 s until the photostationary state was reached. Similarly, photoisomerization studies were individually conducted on 10 μM solution of compounds **2** and **3** in DMSO by UV−vis spectroscopy upon photoillumination at ∼330 nm. In both cases, the distamycin band appeared at ∼306 nm overlapped with the 330 nm $\pi-\pi^*$ absorption band of the −N=N− group, and a less intense n−π^* band appeared at around 370 nm (Figure 2B,C). During photoisomerization, the $\pi-\pi^*$ absorption bands for both ligands at 330 nm decreased along with the distamycin absorption band at ∼306 nm. For compound **2**, all curves passed through common points at 280 and 346 nm during 1 h irradiation (Figure 2B). Irradiation for a period longer than 1 h shifted the common point at 280 to 274 nm. Importantly, throughout the isomerization process, each sample maintained an apparent isosbestic point at ∼346 nm, and monotonous absorption enhancement was observed for the n−π^* transition at ∼380 nm. Photoillumination beyond 5 h, however, resulted in a loss of isosbestic point at 346 nm. So, photoisomerization might have led to different isomerized products that remain in an apparent equilibrium. Similarly, photoillumination of a 10 μM DMSO solution of conjugate **3** up to ∼130 min resulted in both a decrease and blue shift of the $\pi-\pi^*$ absorption intensity at ∼308 nm and enhancement of the n−π^* absorption band intensity at ∼370 nm via an apparent isosbestic point at ∼343 nm as shown

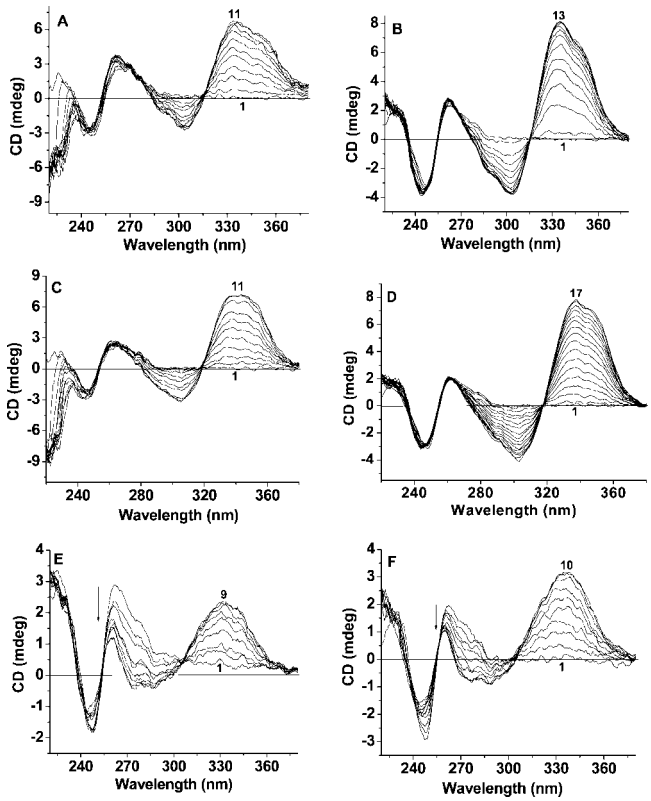

Figure 5. CD titration curves due to **1** in trans form (A), **1*** in cis form (B), **2** in trans form (C), **2*** in ~8/2 (trans/cis) isomeric form (D), **3** in trans form (E), **3*** in ~8/2 (trans/cis) isomeric form (F) carried out with 20 μM poly[d(A-T).d(T-A)] in 10 mM Tris-HCl, 150 mM NaCl, 0.1 mM EDTA at pH 7.4 at 25 °C. For all the panels, trace 1 corresponds to the CD spectrum of poly[d(A-T).d(T-A)] DNA alone. Addition of DNA enhances the ICD band at ~334 nm. Traces 9−11, 13, and 17 signify the corresponding saturation at a given [ligand]/poly[d(A-T).d(T-A)] ratios. No significant change in DNA band was observed for panels A to D upon ligand addition into a given DNA solution. In panels E and F, the down arrow indicates the decrease in DNA band with increasing ligand concentration.

in Figure 2C. Overall, the ligand **3** required ~2 h to reach the photostationary state.

Photoisomerization followed by ^{1}H NMR Spectroscopy. ^{1}H NMR spectroscopy is a very useful technique to determine the cis and trans composition of the ligands in the photostationary state. The changes in ^{1}H NMR spectra of 1 mM solution of **1**, **2**, and **3** in d_6-DMSO upon photoillumination at the respective wavelengths, after periodic time intervals of irradiation, are shown in Supporting Information Figure S4 and Figures 3 and 4. Irradiation of **1** for ~10 min completely shifts 3,3′,5,5′-*H*s (meta protons of azobenzene at ~7.1 ppm) and 2,2′,6,6′-*H*s (ortho protons of azobenzene at ~7.8 ppm) upfield at ~6.8 and ~6.86 ppm, respectively (Supporting Information Figure S4) as verified from reported observations (*35*). Compound **1** required ~10 min to reach the photostationary state with ~100% cis isomeric form. Similarly, upon photoillumination for ~1 h for symmetrical carboxamido-substituted azobenzene derivative, **2** the downfield protons of the azobenzene unit at ~7.9 ppm and ~8.0 ppm shifted upfield as doublets at ~7.7 ppm and ~6.9 ppm, respectively (Figure 3). Analysis of the integration after 3.5−4 h of irradiation revealed that only ~20% of the trans form has been converted into the cis form in the photostationary state. Similar characteristic features were also seen with the carboxamido ligand, **3** (Figure 4). However, unlike in **2** here the photostationary state was reached after 1.5 h, with a composition of ~8:2 (trans/cis) form.

The electronic character of the azobenzene in **1** is different from that in **2** and **3**. In **1**, the substituent is electron-donating, whereas in **2** and **3**, the substituent is electron-withdrawing. It is known both experimentally (*47, 48*) and theoretically (*49, 50*) that the electron-donating substituents render azobenzene susceptible to ready photoisomerization. The nature of spacer that connects distamycin with the azobenzene nucleus is also important. Thus, in **2**, the spacer is protonated, while in **3**, the sites of protonation are at the termini of the oligopeptide chains and not at the spacer unit. This explains why the isomerization is slower in **2** compared to **3**.

DNA Binding Properties. In order to assess the duplex DNA binding properties of each of these conjugates, circular dichroism spectroscopy, thermal melting, and Hoechst displacement assay were employed. For CD experiments, we carried out titration by adding different photoisomeric forms of each conjugates into the fixed (20 μM) poly[d(A-T).d(T-A)] solution in NaCl buffer, and the respective results are shown in Figure 5. The DNA binding properties of these conjugates were investigated starting with 4,4′-substituted bis-alkoxy derivative, **1** and **1***, to the bis-carboxamido-substituted long spacer based **2** and **2*** and short spacer based **3** and **3*** azobenzene−distamycin conjugates (where * indicates the photoirradiated form of the ligands at their respective photostationary states). To understand the mode of binding of azobenzene−distamycin conjugates with duplex DNA, the strength of ligand−DNA interactions were also assessed using molecular docking studies.

A. Circular Dichroism Spectral Titrations. We used circular dichroism spectroscopy to characterize the binding of azobenzene−distamycin conjugates both in their ground state and photoirradiated form to the duplex poly[d(A-T).d(T-A)]. Figure 5A−F shows the circular dichroism spectra from 220 to 380 nm obtained by incremental addition of individual conjugates into the fixed poly[d(A-T).d(T-A)] solution. CD measurements of each ligand with poly[d(A-T).d(T-A)] yielded a set of curves showing two pairs of bands. The intense negative and positive bands observed at 245 and 260 nm arise from the DNA molecule (intrinsic CD). The negative and positive CD bands centered at 303 and 336 nm arise solely from the induction of optical activity of the DNA-bound nonchiral azobenzene−distamycin hybrid molecule (extrinsic or induced CD) (*50*). The induced CD (ICD) values at 336 nm were plotted with the increase [ligand]/[DNA] ([D]/[P]) ratio to evaluate the extent of ligand−DNA interaction and saturation [D]/[P] ratio.

The parent distamycin derivative, **Dist-1**, required a [D]/[P] ratio of 0.2 to "saturate" DNA binding on its minor grooves. This corresponds to 2:1 binding mode, where two **Dist-1** ligands occupy five base pairs along the DNA minor groove (*21*).

During CD titration, there exists an equilibrium between the free ligand in solution and ligand bound to duplex DNA. With increasing DNA affinity of the ligand, the concentration of "free ligand" in solution will be lower. On comparing the binding affinity between trans and cis forms of ligand **1** (Figure 5A vs B), we see from the CD titration that the cis form of the ligand requires a lower concentration (saturation point or maximum ICD intensity at [D]/[P] ratio of 0.2) to cover most of the AT-base pairs along the duplex DNA minor groove than the corresponding trans form (saturation point or maximum ICD intensity at [D]/[P] ratio of 0.3) (Figure 6A). This indicates that at a comparable ligand concentration more trans form of ligand **1** remains free in solution as compared to the cis form in the presence of a fixed DNA concentration. This shows that binding of the cis form of ligand **1** is higher than that of the trans form.

An ICD enhancement at 336 nm was also observed with the ~8/2 (trans/cis) isomeric form of **2*** compared to the 100% trans form of **2** (Figure 5C vs D). The CD titration of **2** required ~0.47 [D]/[P] ratio, while ~8/2 (trans/cis) isomeric mixture of

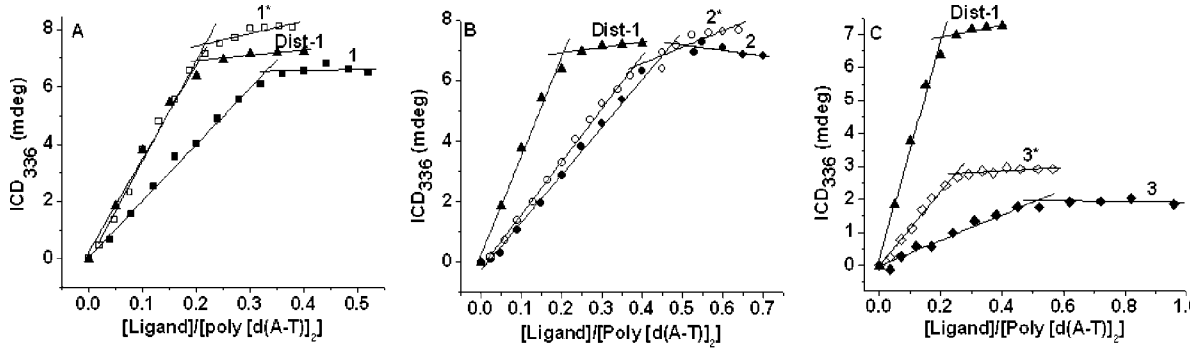

Figure 6. Changes in ICD intensities at 336 nm due to photoisomeric forms of ligands **1** (A), **2** (B), and **3** (C) during titration with 20 μM poly[d(A-T).d(T-A)] in 10 mM Tris-HCl, 150 mM NaCl, 0.1 mM EDTA buffer at pH 7.4 at 25 °C in dark condition. Different isomeric compositions of the ligands are as follows: **1** (∼100% trans), **1*** (∼100% cis), **2** (∼100% trans), **2*** (∼8/2 (trans/cis)), **3** (∼100% trans), and **3*** (∼8/2 (trans/cis)). Distamycin analogue, **Dist-1**, has also been included for comparison.

Table 2. Melting Temperatures (T_m), Apparent Binding Constants (K_{app}), and Saturation [D]/[P] Ratios Obtained from Binding of Dist-1 and Different Forms of 1, 2, and 3 with Poly[d(A-T).d(T-A)]

DNA + ligands	T_m (°C)[a]	ΔT_m (°C)[b]	$K_{app} \times 10^{-5}$ (M^{-1})[c]	[D]/[P]
Poly[d(A-T). d(T-A)] alone	64.7	−		
+ **Dist-1**	67.4	2.7	6.5	0.2
+ **1**	74.0	9.3	7.2	0.3
+ **1***	75.0	10.3	7.4	0.2
+ **2**	81.0	16.3	6.4	0.47
+ **2***	81.9	17.2	7.0	0.37
+ **3**	85.7	21.0	6.8	0.5
+ **3***	86.7	22.0	10.4	0.25

[a] T_m indicates the average melting temperature value of two independent melting experiments that has been done with the complexes of poly[d(A-T).d(T-A)] in the presence of different ligands in 150 mM NaCl, 10 mM Na_2HPO_4, 0.1 mM EDTA, pH = 7.4, at the saturated [D]/[P] ratio. The error is within ±0.2 °C. [b] ΔT_m corresponds to the difference in T_m between DNA alone and DNA−ligand complexes. [c] K_{app} = apparent binding constant obtained from Hoechst displacement assay.

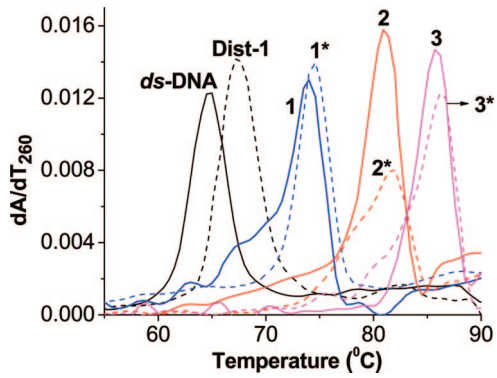

Figure 7. Thermal melting of 20 μM poly[d(A-T).d(T-A)] complexed with various azobenzene−distamycin ligands in NaCl buffer at saturating [D]/[P] ratios. The label of each curve corresponds to DNA: 20 μM poly[d(A-T).d(T-A)]. **Dist-1**: Distamycin analogue, at [D]/[P] = 0.2; **1** and **1*** at [D]/[P] = 0.3 and 0.2; **2** and **2*** at [D]/[P] = 0.47 and 0.37; **3** and **3*** at [D]/[P] = 0.5 and 0.25, respectively.

2* required 0.37 [D]/[P] ratio to saturate ligand binding on DNA minor grooves (Figure 6B). This improvement in ICD intensity and [D]/[P] ratio suggests higher binding of **2*** compared to **2**. A more significant improvement in ICD intensity at 336 nm was observed with the ∼8/2 (trans/cis) isomeric form of **3*** compared to **3** (Figure 5E vs F). The CD titration of 100% trans form of **3** required ∼0.50 [D]/[P] ratio, while ∼8/2 (trans/cis) isomeric mixture of **3*** required only 0.25 [D]/[P] ratio to saturate ligand binding on the DNA minor groove (Figure 6C).

B. Competition for DNA Minor Groove. The apparent binding constants of each ligand toward ds-DNA were evaluated by estimating their efficiency in replacing fully bound Hoechst 33258 from minor grooves of ds-DNA in NaCl buffer. In contrast to CD results, a subtle difference in apparent binding constant values between **1** and **1*** was not apparent from Hoechst displacement assay (Table 2). This is, however, not too surprising, as the binding constant of Hoechst 33258 to the minor groove of ds-DNA is considerably greater than that of distamycin. Interestingly, however, both isomeric forms of **1** rapidly quenched Hoechst fluorescence preferably when 50% of Hoechst was displaced from the duplex DNA minor groove (Supporting Information Figure S5). On the other hand, **2** and **2*** possessed comparable binding constants and manifested a similar type of Hoechst displacement curves (Supporting Information Figure S5). However, a significant difference in ICD intensity observed with **3** and **3*** correlates well with the lower concentration required by **3*** to remove Hoechst from the DNA minor grooves than that of **3**. This fact explains the significant difference in their apparent binding constant values ($K_{app} = 6.8 \times 10^{-5}$ M^{-1} and 10.4×10^{-5} M^{-1}) between the ground and photoisomerized forms of **3** (Supporting Information Figure S5 and Table 2).

C. Influence on DNA Melting. The thermal DNA melting experiment is an important method for the determination of the stability of ligand−ds-DNA complexes. It is known that minor groove binders like distamycin enhance the helix-to-coil transition temperature via recognition of AT-specific bases of ds-DNA (*19*). Here, the thermal denaturation experiments with all ligand−DNA complexes were performed at saturating [D]/[P] ratio in NaCl buffer by following the absorbance change at 260 nm with increase in temperature (Figure 7, Table 2). Importantly, the DNA melting experiment at the saturated [D]/[P] value for each ligand allows us to compare the duplex stability imposed by various alkoxy- and carboxamido-substituted azobenzene distamycin analogues.

The ligand-saturated DNA complexes of both irradiated and non-irradiated solutions of ligand **1** were found to stabilize ds-DNA almost to the same extent. The photoirradiated forms of **1** stabilize ds-DNA by ∼1 °C from that of its ground state. However, they were found to stabilize duplex DNA by ∼7.1 °C more compared to the distamycin analogue, **Dist-1** (Figure 7, Table 2). Such higher T_m for conjugate **1** indicates that a greater number of hydrogen bonding interactions together with other noncovalent interactions (hydrophobic, electrostatic, van der Waals) are responsible for the stabilization of such ligand−DNA complexes. Similarly, the ligand **2** and photoisomerized **2*** stabilized the duplex poly[d(A-T)]$_2$ to 81 and 81.9 °C, respectively, (i.e., by ∼14.5 °C more compared to distamycin analogue, **Dist-1**). The photoisomeric forms of **3** stabi-

Table 3. Free Binding Energies (Δ*G*), Docked Energies, and the Close Contact Distances of Amide Bond of Ligand with DNA Bases Obtained From *Autodock* Calculations of Dist-1, Dist-2, Hoechst, 1, 2, and 3 Ligands with Modeled Duplex [d(GC(AT)$_{10}$CG)]$_2$ DNA[a]

ligands	Δ*G* (kcal/mol)[b]	docked energies (kcal/mol)	closest distances between ligand and DNA bases (Å)	D1 (Å)	D2 (Å)
Dist-1	−7.0	−11.3	2.50, 2.74, 2.32, 2.54	-	-
Dist-2	−7.1	−11.5	2.21, 2.39, 2.53, 2.52, 2.11	-	-
Hoechst	−12.1	−13.0	2.26, 2.18	-	-
1a	−8.2	−21.9	3.35, 5.29, 6.54, 2.74, 4.61, 5.63	11.62	21.53
1b	−7.9	−21.6	3.49, 5.25, 5.78, 2.58, 2.92, 3.69, 4.85, 4.30, 2.56	8.02	14.06
2a	−10.3	−22.7	5.04, 6.61, 5.16, 3.56, 3.19, 5.62, 4.15, 4.24, 3.46	11.91	19.40
2b	−9.8	−22.3	4.14, 2.71,4.27, 3.86, 3.16, 3.49, 3.95, 2.56, 4.56, 3.98	8.17	11.91
3a	−12.9	−24.1	2.94, 4.87, 6.59, 2.61, 3.06, 2.56, 2.51	11.91	17.05
3b	−14.1	−25.3	2.39, 3.06, 2.73, 2.38, 4.65, 5.51, 4.90, 3.51, 2.17, 3.25	7.53	8.30

[a] The D1 and D2 are the distances in Å between azobenzene and linker containing azobenzene moiety of the ligands as shown in Scheme 4. [b] The values obtained by rigid docking of the lowest docked conformation of the ligands initially obtained from the flexible docking studies.

Scheme 4. Schematic Representation of D1 and D2 Distances in the trans and cis Azobenzene−Distamycin Conjugates[a]

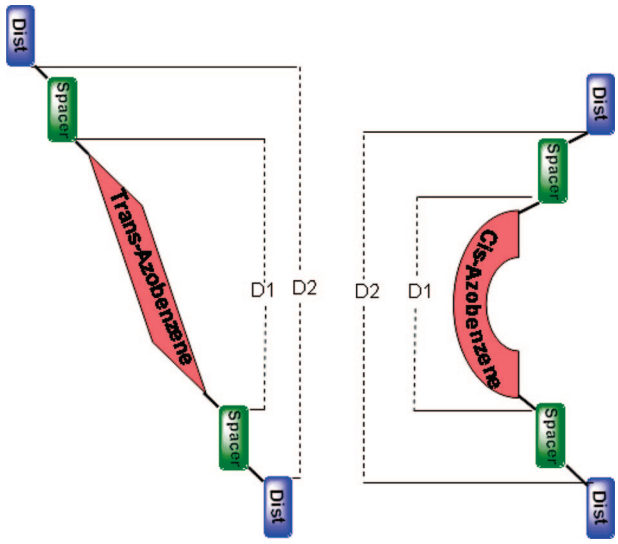

[a] Here, D1 represents the length of azobenzene, and D2 represents the length of azobenzene along with the spacer.

lized duplex poly[d(A-T).d(T-A)] to 85.7 and 86.7 °C, respectively, and ∼18−19 °C more compared to distamycin analogue, **Dist-1** (Figure 7, Table 2). It may be noted that in all cases the ΔT_m and the apparent binding constants (K_{app}) were higher for the photoirradiated forms of the conjugates even if they were small. Importantly, however, the ΔT_m was always achieved with photoirradiated forms of the conjugates at lower [D]/[P] ratio than the respective trans form.

We have also carried out the melting experiment with duplex poly[d(A-T).d(T-A)] in the presence of each ligand including their photoilluminated forms at a fixed [D]/[P] ratio of 0.5, which bring out the differences between trans and cis isomeric forms more clearly. Thus, at this [D]/[P] ratio of 0.5, while **1** stabilized poly[d(A-T).d(T-A)] by 11.5 °C, **1*** afforded a stabilization of 13.3 °C (Supporting Information Table SI-2). Similarly, under the same conditions, photoisomerized **2***and **3***, respectively, brought about 2.4 °C and >1 °C higher stabilization of poly[d(A-T).d(T-A)] than **2** and **3**. These results demonstrate greater stabilization of DNA by the photoisomerized forms of the distamycin−azobenzene conjugates. Hence, the cis form of the conjugates possess higher affinity toward duplex DNA.

D. Molecular Docking on DNA Duplex. To rationalize the experimental trends quantitatively using molecular modeling, initially a rigid docking of the optimized ligand structures with modeled duplex d[GC(AT)$_{10}$CG]$_2$ DNA were performed by *AUTODOCK* v 3.05 (*42*) However, favorable hydrogen bonding interactions between ligand and DNA bases obtained at this level did not adequately explain the experimental results. So, either one side or both sides of the linker atoms were chosen as rotable units for flexible docking of ligands. Finally, a rigid docking was performed with the lowest docked conformation obtained from the flexible docking studies. Such lowest docked conformations of different ligand−DNA complexes were considered for discussion below. The corresponding docking energies and free binding energies (Δ*G*) of all types of rigid and flexible dock conformations of ligand−DNA complexes are shown in Table 3 and Supporting Information Table SI-1. The docked energies and binding energies obtained from the molecular docking studies correlated well with the thermal melting values, as the stabilization of the overall ligand−DNA complexes is influenced by hydrogen bonding and other noncovalent interactions. The binding energies obtained from PreDICCTA (*52*) by supplying the experimental ΔT_m values were similar to these results.

A rigid docking of the **Dist-1** gave a binding free energy of −7.0 kcal/mol (Table 3). There are four hydrogen bonding contacts between the pyrrole amide bond of **Dist-1** and A/T base pairs of DNA in addition to the other noncovalent interactions with the oxo group of the ribose sugar moiety (Figure 8). The DNA base-pair recognition efficiency of **Dist-1** as obtained from the saturation [D]/[P] ratio is supported by the number of hydrogen bonding contacts.

The docking of **1**, **2**, and **3** showed that the azobenzene moiety allows both the distamycin arms to satisfy the extended mode of binding (*11*) unlike the hairpin conformation as observed with γ-amino butyric acid linker based distamycin derivatives (*53*). The isomer **1b** has more pyrrole amide bonds available for hydrogen bonding with the AT base pairs than **1a**. This was supported by higher ICD intensity and low [D]/[P] ratio of **1*** than **1** (Figure 6A, Table 2). One or both benzene moieties of the planar azobenzene group in the trans form (**1a**) approach the ds-DNA to be involved in hydrophobic interactions with the DNA bases. In addition, with long spacer (∼11 Å), the number of pyrrole amides that are able to form hydrogen bonds with the DNA bases decreases, while the nonplanar azobenzene moiety in the cis form prefers to remain out of the DNA helical surface and thus allow more pyrrole amide bonds to satisfy hydrogen bonding interactions with DNA bases (not shown).

The better hydrogen bonding contacts of the para-substituted **1b** over **1a** can also be explained by the difference in D1 and D2 distances. D1 corresponds to the length of azobenzene and D2 represents D1 and spacer length (Scheme 4). The D2 distance varies in the ligands due to variation of electron-donating vs electron-withdrawing substituent of the azobenzene moiety (**1, 2**) and also due to the existing spacer in **Dist-1** and **Dist-2** (Figure 1). In the case of trans to cis photoisomerization of **1**, the lowest-energy docked conformation has D1 = ∼3.5 Å and an overall decrease of D2 from 21.53 Å to 14.06 Å leading to an increase in hydrogen bonds (Table 3). The docked (−21.9 and −21.6 kcal/mol) and free binding energies (−8.2 and −7.9 kcal/mol) are in tune with the melting temperature values (Table 3). The subtle differences in docked and free

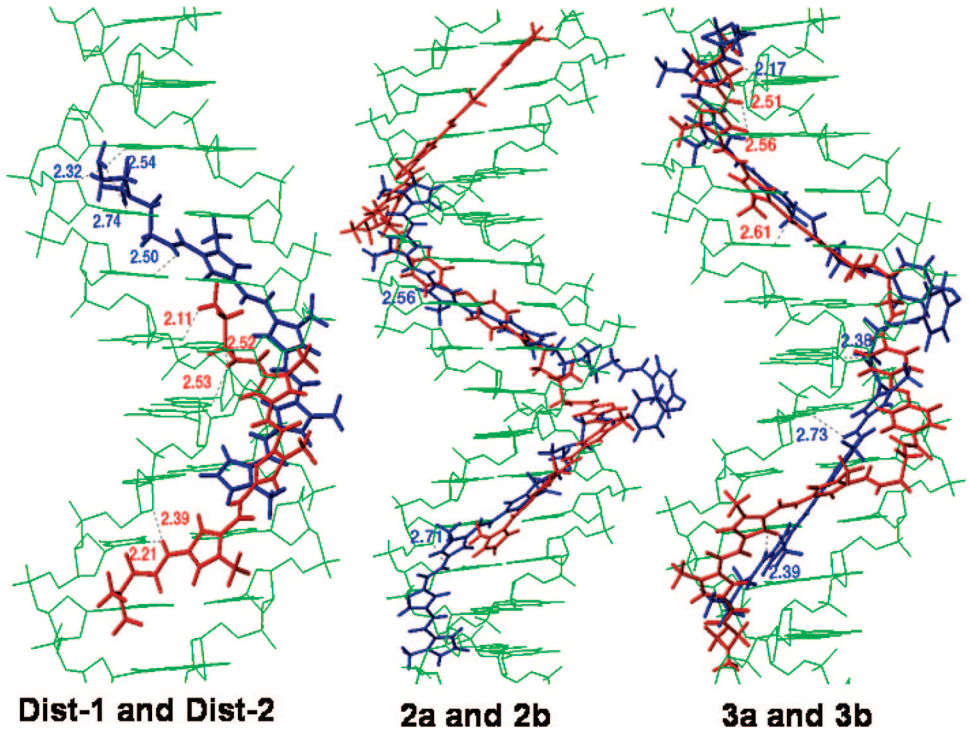

Figure 8. The docked conformations of **Dist-1**, **Dist-2**, and both isomeric forms of the ligands **2** and **3** with duplex d[GC(AT)$_{10}$CG]$_2$ DNA scaffold are shown. Ligand, **Dist-1**, and cis form of ligands **2b** and **3b** are shown in blue-colored capped sticks, whereas **Dist-2** and trans forms of ligand **2a** and **3a** are shown in red-colored capped sticks. The image is from *Sybyl 7.0* (*54*).

binding energies between **1a** and **1b** support the low variation in melting temperature at saturating [D[/[P] ratio and apparent binding constant (K_{app}) values. This explains the DNA binding features of the dialkoxy azobenzene−distamycin dimers **1a** and **1b**.

In the case of dicarboxy azobenzene−distamycin conjugatees also, the docked conformations of **2b** with ds-DNA show greater availability of the hydrogen bond contacts between pyrrole amide bonds and AT base pairs over **2a** (Figure 8, Table 3) as observed from the CD spectral titrations. As seen in **1a** and **1b**, a similar large variation of D1 = ∼3.7 Å around the azobenzene moiety and contraction of D2 from 19.4 Å to 11.91 Å, where D2 = [-$(CH_2)_2$NMe$(CH_2)_2$NHOCPhN═NPhCONH$(CH_2)_2$NMe-$(CH_2)_2$-], are observed during trans to cis photoisomerization (Table 3). This might cause a subtle improvement in [D]/[P] ratio of **2*** than that of **2**. The comparative binding constant values are proportional to that of **Dist-1**, as possible hydrogen bonding contacts seem to be similar for both cases (Table 3). The improved T_m values compared to **1** and **1*** can again be correlated with the higher docking (−22.7 and −22.3 kcal/mol) and free binding energies (−10.3 and −9.8 kcal/mol), as hydrogen bonding interactions together with other noncovalent interactions contribute to stabilizing the ligand−DNA complexes. Smaller differences in docking and free binding energies between both photoisomeric forms of **2** again quantify their small variation in both melting temperature and K_{app} values.

The docked conformation of **3b** has shown a larger number of hydrogen bonding contacts with DNA bases compared to **3a** (Figure 8). The trans to cis isomerization of **3** has shown a decrease in the length of D1= ∼4.4 Å around the azobenzene moiety and simultaneous contraction of D2 from 17.05 Å to 8.3 Å along the linker length containing the azobenzene moiety (Scheme 4, Table 3). This helps both distamycin arms in **3b** to align along the isohelical pitch of the DNA helical axis, which achieves a maximum number of hydrogen bonding contacts and favorable electrostatic interactions with DNA in comparison to **3a** (Table 3). These observations support higher ICD intensity, lower [D]/[P] ratio, and higher K_{app} value for **3*** than **3**. A higher apparent binding constant value of the photoirradiated form of **3** may be a consequence of its higher free binding energy of −14.1 kcal/mol compared to free binding energy of Hoechst 33258 (−12.1 kcal/mol). This implies that a greater difference in DNA binding affinity and apparent DNA binding constant between the ∼8/2 (trans/cis) isomeric form and the trans form can be achieved with short linker based conjugate, **3**, compared to the flexible, long linker based ligand **2**. Photoisomerization of azobenzene induced a greater change of D2 in **3** compared to the docked conformations of **1** and **2** (Table 3). This eventually caused a greater difference in DNA binding affinity between **3** and **3*** compared to both isomeric forms of **1** and **2**. Further, the shape of **3b** was found to be more appropriately matched with the DNA helical axis (Figure 8). Even the positive charge at the N-terminal position is relatively more freely available for electrostatic interaction with the phosphates of DNA. This in fact contributed to enhancing the ligand−DNA interaction of **3** compared to other ligands (**1**, **2**).

CONCLUSIONS

The combined experimental data established how distamycin binding on DNA minor grooves was influenced by the presence of an azobenzene core. From ^{1}H NMR and UV−vis spectroscopy, it has been found that the nature of the substituent with respect to the core azobenzene unit (**1** vs **2**) and the linker lengths between distamycin and azobenzene unit (**2** vs **3**) influence the rate and the extent of azobenzene isomerization. Thus, the DNA binding properties of such conjugates were found to directly depend on the orientation of the distamycin with respect to the azobenzene core linker length between azobenzene and distamycin moiety and on the position of positive charge along the oligopeptide backbone. The azobenzene core influenced the conformational freedom of the oligopeptide largely, thereby preventing favorable isohelical orientation of the distamycin units along the ds-DNA minor grooves. Thus, at room temperature, geometrical features of the

azobenzene core prevent simultaneous participation of both distamycin arms in an optimal DNA recognition process. This was manifested by a less intense ICD band and the requirement of high [ligand]/[DNA] ratio to saturate minor groove binding by azobenzene−distamycin hybrids compared to the distamycin alone. According to the results obtained from CD spectroscopy, the photoirradiated forms **1***, **2***, and **3*** favored DNA binding affinity compared to the corresponding trans form as evidenced from high ICD_{336} intensity and low [D]/[P] values for the cis form of the ligands.

Molecular docking studies indicate that during photoisomerization the difference in planarity of the azobenzene moiety together with the change in the length either around the azobenzene moiety (D1) or along the linker containing the azobenzene moiety (D2) determines the orientation of both distamycin arms along the DNA minor groove surface. This eventually causes a greater number of hydrogen bonding contacts between the pyrrole amide and the DNA bases in their cis geometry compared to that in the trans configuration. For example, a greater difference in D2 during photoisomerization for the short spacer based azobenzene−distamycin conjugates explains the relatively larger difference in the ICD intensity and the DNA binding constant values between **3** and **3***. CD spectra allowed measurements of the differences in the DNA binding affinity between trans and photoirradiated form of all the ligands. This was not, however, possible with the Hoechst displacement assay. Except for ligand **3**, there was very little difference in the apparent binding constant values between the isomeric forms of other ligands. This could be due to lower binding free energies of these ligands (**1a**, **1b**, **2a**, and **2b**) compared to Hoechst 33258 as a MGB. As expected, all the dimeric distamycin−azobenzene conjugates were able to stabilize polymeric alternating A/T-rich duplex DNA more effectively compared to the monomeric distamycin analogue, **Dist-1**. There is a gradual increase in the overall stability of DNA−ligand complexes as we move from **1a** to **3a**. Although no major differences in T_m values were observed between the conjugates before and after photoillumination at "saturating" [D]/[P] ratio based on ICD titration data, there was a perceptible increase in T_m values when DNA melting was performed at a constant [D]/[P] ratio of 0.5 with each ligand. This indicates that the cis isomeric forms of such conjugates stabilize ds-DNA more than their trans counterparts at a fixed ligand/DNA ratio.

Experimental and theoretical studies of DNA binding with ligands (**1**, **2**, and **3**) demonstrate the role of linker length between azobenzene and distamycin conjugates for achieving favorable DNA binding affinity and a perceptible difference in duplex DNA binding affinity during photoisomerization. Thus, it was possible to regulate distamycin binding on ds-DNA to some extent by properly anchoring a photoactive disubstituted azobenzene unit to the oligopeptide backbone using a short and rigid spacer.

In summary, the present study describes how specific alterations in a set of azobenzene−distamycin conjugates alter their molecular structure and geometry, which in turn influences their DNA binding affinity on the floor of the minor groove. This also gives significant leads for the design of MGBs, with structural prerequisites to selectively control DNA recognition in the presence of external stimulus. Such an approach reveals a way to control certain biological events where one can regulate the binding specificity and efficiency of small molecules on duplex DNA with light.

ACKNOWLEDGMENT

We thank the Department of Biotechnology, Government of India for funding this work. We also thank Centre for Modeling, Simulation and Design (CMSD), and High Performance Computing Facility (HPCF), University of Hyderabad, Maui High Performance Computing Center (MHPCC) at Hawaii and the Supercomputer Education and Research Centre (SERC) of Indian Institute of Science for computational facilities. D.U.R. and S.D. acknowledge CSIR for senior research fellowships.

Supporting Information Available: Spectral characterization data of the final compounds **1**−**3** and the optimized coordinates of all the ligands and the docked energies for rigid docking details. This material is available free of charge via the Internet at http://pubs.acs.org.

LITERATURE CITED

(1) Bailly, C., and Chaires, J. B. (1998) Sequence-specific DNA minor groove binders. Design and synthesis of netropsin and distamycin analogues. *Bioconjugate Chem. 9*, 513–38.

(2) Dervan, P. B. (2001) Molecular recognition of DNA by small molecules. *Biorg. Med. Chem. 9*, 2215–35.

(3) Wemmer, D. E., and Dervan, P. B. (1997) Targeting the minor groove of DNA. *Curr. Opin. Struct. Biol. 7*, 355–61.

(4) Bruice, T. C., Mei, H., He, G., and Lopez, V. (1992) Rational design of substituted tripyrrole peptides that complex with DNA by both selective minor-groove binding and electrostatic interaction with the phosphate backbone. *Proc. Natl. Acad. Sci. U.S.A. 89*, 1700–04.

(5) Buchmueller, K. L., Staples, A. M., Howard, C. M., Horick, S. M., Uthe, P. B., Le, N. M., Cox, K. K., Nguyen, B., Pacheco, K. A. O., Wilson, W. D., and Lee, M. (2005) Extending the language of DNA molecular recognition by polyamides: unexpected influence of imidazole and pyrrole arrangement on binding affinity and specificity. *J. Am. Chem. Soc. 127*, 742–50.

(6) Trauger, J. W., Baird, E. E., Mrksich, M., and Dervan, P. B. (1996) Extension of sequence-specific recognition in the Minor Groove of DNA by pyrrole-imidazole polyamides to 9−13 base pairs. *J. Am. Chem. Soc. 118*, 6160–66.

(7) Streltsov, S. A., Gromyko, A. V., Oleinikov, V. A., and Zhuze, A. L. (2006) The Hoechst 33258 covalent dimer covers a total turn of the double-stranded DNA. *J. Biomol. Struct. Dyn. 24*, 285–302.

(8) Correa, B. J., Canzio, D., Kahane, A. L., Reddy, P. M., and Bruice, C. T. (2006) DNA sequence recognition by Hoechst 33258 conjugates of hairpin pyrrole/imidazole polyamides. *Bioorg. Med. Chem. Lett. 16*, 3745–50.

(9) Joubert, A., Sun, X., Johansson, E., Bailly, C., Mann, J., and Neidle, S. (2003) Sequence-selective targeting of long stretches of the DNA minor groove by a novel dimeric bis-benzimidazole. *Biochemistry 42*, 5984–92.

(10) Buchmueller, K. L., Staples, A. M., Howard, C. M., Horick, S. M., Uthe, P. B., Le, N. M., Cox, K. K., Nguyen, B., Pacheco, K. A. O., Wilson, W. D., and Lee, M. (2004) Extending the language of DNA molecular recognition by polyamides: Unexpected influence of imidazole and pyrrole arrangement on binding affinity and specificity. *J. Am. Chem. Soc. 127*, 742–50.

(11) Trauger, J. W., Baird, E. E., and Dervan, P. B. (1998) Recognition of 16 base pairs in the minor groove of DNA by a pyrrole-imidazole polyamide dimer. *J. Am. Chem. Soc. 120*, 3534–35.

(12) Woods, C. R., Ishii, T., Wu, B., Bair, K. W., and Boger, D. L. (2002) Hairpin versus extended DNA binding of a substituted beta-alanine linked polyamide. *J. Am. Chem. Soc. 124*, 2148–52.

(13) Chaudhuri, P., Ganguly, B., and Bhattacharya, S. (2007) An experimental and computational analysis on the differential role of the positional isomers of symmetric bis-2-(pyridyl)-1*H*-benzimidazoles as DNA binding agents. *J. Org. Chem. 72*, 1912–23.

(14) Chaudhuri, P., Majumder, H. K., and Bhattacharya, S. (2007) Synthesis, DNA binding, and *Leishmania* topoisomerase inhibition activities of a novel series of anthra[1,2-d]imidazole-6,11-dione derivatives. *J. Med. Chem. 50*, 2536–40.

(15) Bhattacharya, S., and Mandal, S. S. (1995) Ambient oxygen activating water soluble cobalt-salen complex for DNA cleavage. *J. Chem. Soc. Chem. Commun.* 2489–90.
(16) Bhattacharya, S., and Mandal, S. S. (1996) DNA cleavage by intercalatable cobalt-bispicolylamine complexes activated by visible light. *Chem. Commun.* 1515–16.
(17) Mandal, S. S., Varshney, U., and Bhattacharya, S. (1997) Role of central metal ion and ligand charge in the DNA binding and modification by metallosalen complexes. *Bioconjugate Chem. 8*, 798–812.
(18) Mandal, S. S., Kumar, N. V., Varshney, U., and Bhattacharya, S. (1996) Metal-ion dependent DNA cleavage by transition metal complexes of a new water-soluble salen dereivative. *J. Inorg. Biochem. 63*, 265–272.
(19) Thomas, M., Varshney, U., and Bhattacharya, S. (2002) Distamycin analogues without leading amide at their *N*-termini - comparative binding properties to AT- and GC-rich DNA sequences. *Eur. J. Org. Chem.* 3604–15.
(20) Bhattacharya, S., and Thomas, M. (2001) DNA recognition by the first *tail-to-tail* linked distamycin-like oligopeptide dimers. *Chem. Commun.* 1464–65.
(21) Bhattacharya, S., and Thomas, M. (2000) DNA binding properties of novel distamycin analogs that lack the leading amide unit at the N-terminus. *Biochem. Biophys. Res. Commun. 267*, 139–44.
(22) Ghosh, S., Defrancq, E., Lhomme, J. H., Dumy, P., and Bhattacharya, S. (2004) Efficient conjugation and characterization of distamycin-based peptides with selected oligonucleotide stretches. *Bioconjugate Chem. 15*, 520–29.
(23) Ghosh, S., Usharani, D., De, S., Jemmis, E. D., and Bhattacharya, S. (2008) Photophysical and duplex-DNA-binding properties of distamycins based on 4,4'- and 2,2'-dialkoxyazobenzenes as the core. *Chem. Asian J. 3*, 1949–1961.
(24) Rau, H. *Photochemistry and Photophysics* (Rabek, J. F., Ed.) pp 119−41, Vol. II, CRC, Boca Raton, FL.
(25) Rau, H. (1990) Azo compounds, In *Studies in Organic Chemistry: Photochromism, Molecules and Systems* (Dürr, H., and Bonas-Laurent, H., Eds) pp 165−92, Vol *40*, Elsevier, Amsterdam.
(26) Flint, D. G., Kumita, J. R., Smart, O. S., and Woolley, G. A. (2002) Using an azobenzene cross-linker to either increase or decrease peptide helix content upon trans-to-cis photoisomerization. *Chem. Biol. 9*, 391–97.
(27) Asanuma, H., Liang, X., Yoshida, T., and Komiyama, M. (2001) Photocontrol of DNA duplex formation by using azobenzene-bearing oligonucleotides. *ChemBioChem 2*, 39–44.
(28) Liang, X., Asanuma, H., and Komiyama, M. (2002) Photoregulation of DNA triplex formation by azobenzene. *J. Am. Chem. Soc. 124*, 1877–83.
(29) Dohno, C., Uno, S., and Nakatani, S. (2007) Photoswitchable molecular glue for DNA. *J. Am. Chem. Soc. 129*, 11898–99.
(30) Srivastava, A., Ghorai, S., Bhattacharjya, A., and Bhattacharya, S. (2005) A tetrameric sugar-based azobenzene that gels water at various pH values and in the presence of salts. *J. Org. Chem. 70*, 6574–82.
(31) Guerrero, L., Smart, O. S., Weston, C. J., Burns, D. C., Woolley, G. A., and Allemann, R. K. (2005) Photochemical regulation of DNA-binding specificity of MyoD. *Angew. Chem., Int. Ed. 44*, 7778–82.
(32) Liu, M., Asanuma, H., and Komiyama, M. (2006) Azobenzene-tethered T7 promoter for efficient photoregulation of transcription. *J. Am. Chem. Soc. 128*, 1009–15.
(33) Bhattacharya, S., and Thomas, M. (2000) Facile synthesis of oligopeptide distamycin analogs devoid of hydrogen bond donors or acceptors at the N-terminus: sequence-specific duplex DNA binding as a function of peptide chain length. *Tetrahedron Lett. 41*, 5571–75.
(34) Bhattacharya, S., and Thomas, M. (2001) Facile synthesis of novel fluorescent distamycin analogues. *Tetrahedron Lett. 42*, 5525–28.
(35) Wei, W., Tomohiro, T., Kodaka, M., and Okuno, H. (2000) Selective synthesis and kinetic measurement of 1:1 and 2:2 cyclic compounds containing 1,4,7,10-tetraazacyclododecane and azobenzene units. *J. Org. Chem. 65*, 8979–87.
(36) Ameerunisha, S., and Zacharias, P. S. (1995) Characterization of simple photoresponsive systems and their applications to metal ion transport. *J. Chem. Soc., Perkin Trans. 2*, 1679–82.
(37) Kasha, M. (1948) Transmission filters for the ultraviolet. *J. Opt. Soc. Am. 38*, 929–34.
(38) McGhee, J. D., and Von Hippel, P. H. (1974) Theoretical aspects of DNA-protein interactions: co-operative and non-co-operative binding of large ligands to a one-dimensional homogeneous lattice. *J. Mol. Biol. 86*, 469–489.
(39) Frisch, M. J.; Trucks, G. W. et al. (2003) *Gaussian 03*, Gaussian, Inc., Wallingford, CT.
(40) Nicole, A. T. F. et. al. *AMBER 8*, University of California, San Francisco.
(41) Duan, Y., Wu, C., Chowdhury, S., Le, M. C., Xiong, G., Zhang, W., Yang, R., Cieplak, P., Luo, R., and Lee, T. (2003) A point-charge force field for molecular mechanics simulations of proteins based on condensed-phase quantum mechanical calculations. *J. Comput. Chem. 24*, 1999–2012.
(42) AutoDock 3.05, 10550 North Torrey Pines Road, La Jolla, CA 92037−1000.
(43) Morris, G. M., Goodsell, D. S., Halliday, R. S., Huey, R., Hart, W. E., Belew, R. K., and Olson, A. J. (1998) Automated docking using a Lamarckian genetic algorithm and an empirical binding free energy function. *J. Comput. Chem. 19*, 1639–62.
(44) Evans, D. A., and Neidle, S. (2006) Virtual screening of DNA minor groove binders. *J. Med. Chem. 49*, 4232–38.
(45) Detering, C., and Varani, G. (2004) Validation of automated docking programs for docking and database screening against RNA drug targets. *J. Med. Chem. 47*, 4188–4201.
(46) Chen, K, Adelstein, S. J., and Kassis, A. I. (2004) Molecular modeling of the interaction of iodinated Hoechst analogs with DNA: Implications for new radiopharmaceutical design. *J. Mol. Struct. (Theochem) 711*, 49–56.
(47) Singh, A. K., and Madhusoodnan, K. S. (1998) Effect of substituents and media on photochromic properties of azobenzene systems. *National Academy Science Letters (India) 21*, 243–46.
(48) Angiolini, L., Caretti, D., Giorgini, L., Salatelli, E., Altomare, A., Carlini, C., and Solaro, R. (2000) Optically active polymethacrylates with side-chain L-lactic acid residues connected to push−pull azobenzene chromophores. *Polymer 41*, 4767–80.
(49) Crecca, C. R., and Roitberg, A. E. (2006) Theoretical study of the isomerization mechanism of azobenzene and disubstituted azobenzene derivatives. *J. Phys. Chem. A 110*, 8188–8203.
(50) Diau, E. W. G. (2004) A new trans-to-cis photoisomerization mechanism of azobenzene on the S1 (n,π) surface. *J. Phys. Chem. A 108*, 950–56.
(51) Luck, G., Zimmer, C., Reinert, K. E., and Arcamone, F. (1977) Specific interactions of distamycin A and its analogs with (A-T) rich and (G-C) rich duplex regions of DNA and deoxypolynucleotides. *Nucleic Acids Res. 4*, 2655.
(52) Shaikh, S. A., and Jayaram, B. (2007) A swift all-atom energy-based computational protocol to predict DNA-ligand binding affinity and ΔT_m. *J. Med. Chem. 50*, 2240–44.
(53) Heckel, A., and Dervan, P. B. (2003) U-Pin polyamide motif for recognition of the DNA minor groove. *Chem. Eur. J. 9*, 3353–66.
(54) SYBYL 7.0, Tripos Inc., 1699 South Hanley Rd., St. Louis, MO, 63144.

BC800130U